INVESTIGATION OF THE PERFORMANCE OF A GAS-LOADED VARIABLE CONDUCTANCE HEAT PIPE

Keith Earl Reynolds

NAVAL POSTGRADUATE SCHOOL
Monterey, California

THESIS

INVESTIGATION OF THE PERFORMANCE
OF A GAS-LOADED
VARIABLE CONDUCTANCE HEAT PIPE

by

Keith Earl Reynolds

Thesis Advisor: M. Kelleher

December 1972

Approved for public release; distribution unlimited.

Investigation of the Performance of a Gas-Loaded Variable Conductance Heat Pipe

by

Keith Earl Reynolds
Lieutenant Commander, United States Navy
B.S., United States Naval Academy, 1963

Submitted in partial fulfillment of the
requirements for the degree of

MASTER OF SCIENCE IN MECHANICAL ENGINEERING
and
MECHANICAL ENGINEER

from the

NAVAL POSTGRADUATE SCHOOL

ABSTRACT

A variable conductance heat pipe was designed and constructed to study the performance characteristics of the gas loaded heat pipe with particular emphasis on the effect of gravity. Heat inputs were varied from 10 to 50 watts and the operating position of the heat pipe was varied from horizontal to vertical with the condenser above the evaporator. Condenser temperature profiles are presented for various heat inputs and positions for the conventional and gas loaded heat pipe. The possibility of stratification in a horizontal heat pipe operating with a non-condensible gas that has a larger molecular weight than the working fluid is discussed based on observations presented.

Additionally, a one dimensional analysis was formulated and used to compare with the experimental results. The results show a good agreement between theory and experiment, indicating that the developed mathematical model adequately describes the physical situation.

TABLE OF CONTENTS

LIST OF FIGURES

NOMENCLATURE

A_c	Cross sectional area of vapor space	ft^2
A_p	Cross sectional area of wick-wall combination	ft^2
A_s	Outside surface area of condenser section	ft^2
D	Diameter of vapor space (equals $2R_v$)	ft
g	Gravity	ft/sec^2
h	Heat transfer coefficient	BTU/hr °F ft^2
h_{fg}	Latent heat of vaporization	BTU/lbm
J	Permeability	
k	Thermal conductivity	BTU/hr F ft
L	Length of condenser section	ft
$\dot{m}$	Condensation rate	lbm/ft^2 sec
P	Pressure	lb/ft^2
Q	Heat input	BTU/ft^2 sec
R	Electrical resistance	ohms
R_w	Inside radius of pipe	ft
T	Local vapor space temperature	°R
T_∞	Ambient temperature	°R
V	Voltage	volt
W	Mass ratio of working vapor to total density	
σ	Surface tension	lb/ft
ϕ	Void fraction of wick	
ν	Kinematic viscosity	ft^2/sec

ρ	Density	lbm/ft^3
μ	Dynamic viscosity	$lb\text{-}sec/ft^2$
σ_{12}	Lennard-Jones force constant	ft
Ω_D	Collision integral based on Lennard-Jones potential function	$\frac{{}^\circ K^{3/2} sec}{lbf\ ft^2}$
δ	Distance between wires in screen mesh wick	in

SUBSCRIPTS

a	Working fluid
b	Non-condensible gas
s	Stainless steel
L	Liquid working fluid

ACKNOWLEDGEMENT

The author wishes to take this opportunity to express his appreciation to the many people who made this work possible. A complete list of people to which he is indebted is impossible but it is hoped that by naming a few individuals even those unnamed will know their efforts were appreciated.

Professor M. Kelleher, his thesis advisor, was the real guiding light throughout this research and without his consummate effort this work could not have been completed.

The personnel of the Mechanical Engineering Machine Shop of the Naval Postgraduate School provided timely and invaluable assistance in preparation of the experimental apparatus.

Finally, and most importantly to my wife Sandra, for her patience and devotion through repeated manuscript typings, a most grateful, thank you.

I. INTRODUCTION

A. BACKGROUND

The heat pipe is a device capable of transferring large amounts of heat while operating at a nearly constant temperature. The major development of this device has occurred within the last decade although the original concept was proposed in 1944. This proposal, by R. S. Gaugler [Ref. 1] of the General Motors Corporation, was not acted upon at that time. A similar proposal by L. Trefethen [Ref. 2] was made to the General Electric Company in 1962 but was not investigated. The advent of the space program led to a renewed interest in the heat pipe in 1964 by G. M. Grover et al [Ref. 3] of the Los Alamos Scientific Laboratory. The possibility of developing a reliable, efficient and lightweight heat transfer device for application in space equipment was too appealing to allow the concept to again be overlooked.

B. HEAT PIPE OPERATION

The sealed heat pipe is lined with a capillary wick structure. The vessel is evacuated and partially filled with a fluid referred to as the working fluid. During operation the working fluid is continuously evaporating in one section of the pipe and condensing throughout another section (see Figure 1). The condensate is returned to the evaporator section by means of capillary force acting

through the wick structure. This change of phase process results in a nearly constant temperature throughout the heat pipe. The near isothermal operation of the heat pipe was reported in 1965 by K.F. Bainton [Ref. 4]. The isothermal characteristic of the heat pipe allows for a more efficient heat transfer device than that achieved with an equivalent solid metal rod. An effective thermal conductivity for a lithium heat pipe of 1,000 to 10,000 times that of an equivalent metal rod was reported by workers at RCA in 1967 [Ref. 5].

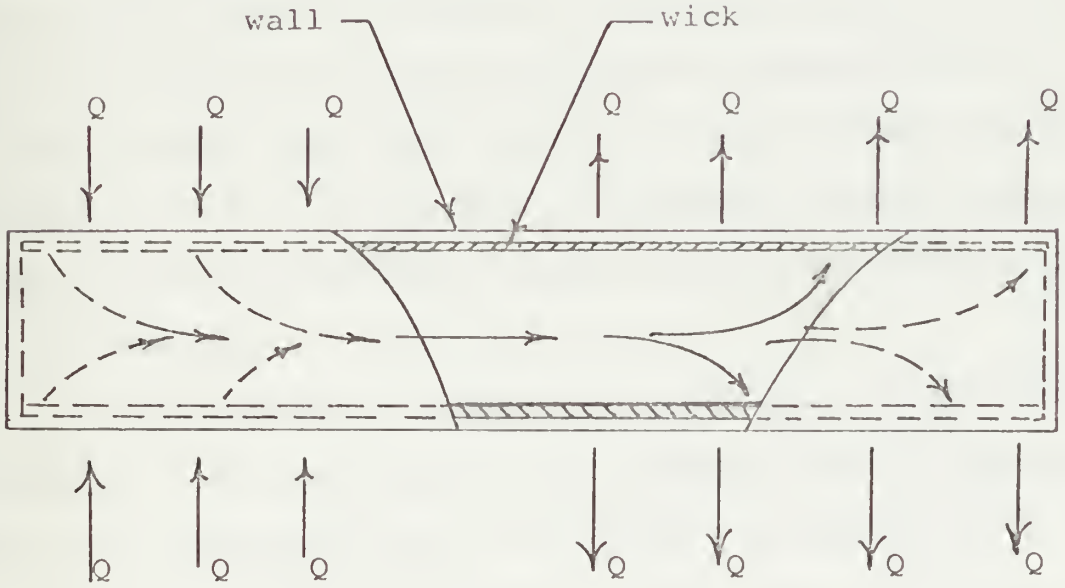

Heat pipe vapor flow diagram
figure 1

The introduction of a non-condensable gas along with the working fluid alters the performance of the heat pipe appreciably. During operation the non-condensable gas is driven to the condenser along with the working vapor.

Unlike the vapor however the gas does not condense and thereby forms a high concentration of the non-condensable gas in a portion of the condenser. As the concentration of the non-condensable gas increases the amount of working fluid present and the condensation rate decrease. The temperature of the pipe in this portion of the condenser will therefore become less than in a portion where the non-condensable gas is absent or is a very small amount of the concentration. Since the pressure of a saturated vapor is directly proportional to its temperature, the amount of working vapor present will decrease with the temperature. For a large enough concentration of non-condensable gas in a portion of the condenser, ambient temperature will be approached. The small amount of working fluid present forming the partial pressure of methanol will not condense, thereby reducing the heat transfer area and the conductance of the heat pipe.

If the evaporator temperature increases, the partial pressure of the working fluid increases thereby compressing the non-condensable gas into a smaller volume which in turn increases the heat transfer area. The pipe's conductance is thereby increased. This characteristic of the gas loaded heat pipe enables it to have the potential to experience smaller operating temperature variations than a conventional heat pipe for similar changes in heat input. Therefore, the process by which the non-condensable gas

collects in the condenser has a direct bearing on the heat pipe's performance.

Two analyses have been developed to give insight into the behavior of the gas loaded heat pipe. The first, the flat front theory, was developed by W. Biemert [Ref. 6]. This theory assumes that during steady state operation of the gas loaded heat pipe the vapor and gas are separated in the condenser by a vertical flat front. The axial heat conduction of the pipe is considered negligible in this theory. The possibility of a pressure gradient being present in the pipe is excluded and diffusion is not considered. With all of these assumptions an analysis of the heat pipe performance is straight forward and proves adequate in the evaluation of several heat pipe parameters. Specifically the volume of the gas reservoir and the ratio of condenser to reservoir volume can be determined. Figure 2 represents the flat front theory.

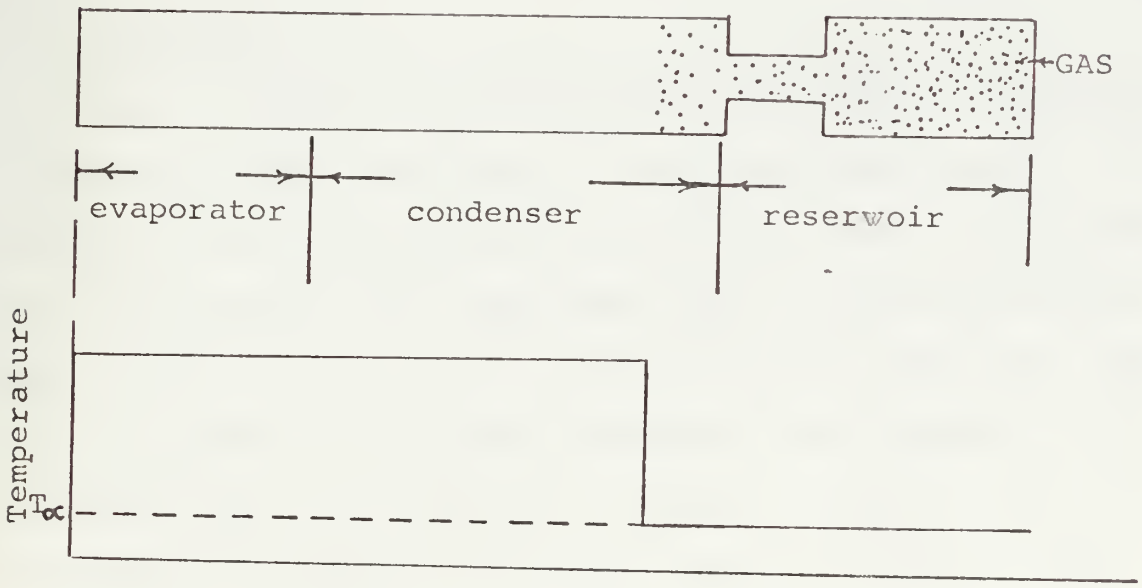

Vapor-gas flat front model

figure 2

More recently, Marcus and Edwards [Ref. 7] have developed the diffuse front theory. In this analysis the contribution of binary diffusion between the non-condensable gas and the working vapor is considered along with axial conduction in the pipe wall. In addition to heat transfer from the condenser by convection the contribution due to radiation is included. The inclusion of these phenomenon results in the vapor-gas interface spreading out into a more realistic profile. This analysis develops accurate temperature and concentration profiles for the condenser section.

This analysis was used to formulate the TRW computer program which is capable of calculating, for various gas loaded heat pipe geometries, among other parameters:

(a) the wall temperature profile;

(b) heat and mass transfer;

(c) gas reservoir size.

C. OBJECTIVE

When a container is filled with two vapors of dissimilar molecular weight the vapor of larger molecular weight will settle to the bottom portion of the container due to gravity. In the operating gas loaded heat pipe the non-condensable gas tends to collect at the end of the heat pipe away from the evaporator, having been convected there along with the working vapor. An inherently unstable situation will therefore be present in the gas loaded heat pipe if the

condenser is above the evaporator and the molecular weight of the non-condensable gas exceeds that of the working vapor. The tendency of the gravitational force is to oppose the convection of the non-condensable gas, thereby spreading out the concentration of the gas. This decrease in the gradient of the working vapor concentration is accompanied by a decrease in the temperature gradient. Therefore, it was the objective of this work to investigate the operation of a gas loaded heat pipe with particular emphasis on the effects of gravity.

The heat pipe used was designed to operate horizontally, vertically with the condenser above the evaporator or any angle in between these two positions. This variation of the angle of operation allowed a variation in the axial component of the gravitational force. The results presented herein are the product of both data obtained from a heat pipe designed and constructed for this purpose and a one dimensional analysis.

II. DESCRIPTION OF EXPERIMENT

A. OVERALL DESIGN

As mentioned earlier the axial conduction of the heat pipe wall tends to spread out the gas vapor interface. To reduce this, the heat pipe was constructed from a stainless steel pipe with a wall thickness of 0.0635 inches. Fins in the form of Acme threads were cut on a lathe along the condenser section to a depth of 0.0255 inches.

One of the two end plates was soldered in place while the other was designed to be easily removed from the condenser end of the heat pipe. The removable end plate, as shown in Figure 3, was in the form of an internally threaded cap. The cap was fastened to a threaded flange which was welded to the end of the heat pipe. An O ring was placed in the flange to effect a pressure and vacuum seal. The condenser end cap was designed with a 0.25 inch diameter tube soldered to its external side. Through a T connection the tube provided the necessary inlet for a pressure transducer, vacuum valve and means of evacuating and filling the heat pipe.

A mesh stainless steel screen around the inside wall of the pipe was used for the wick. To retain the wick firmly against the wall a longitudinal stainless steel spring was inserted along the entire length of the pipe.

The evaporator heating device was a resistance heater made of .125 inch wide, flat Nichrome strip powered by a

direct current power supply. Figure 4 shows the overall design of the heat pipe.

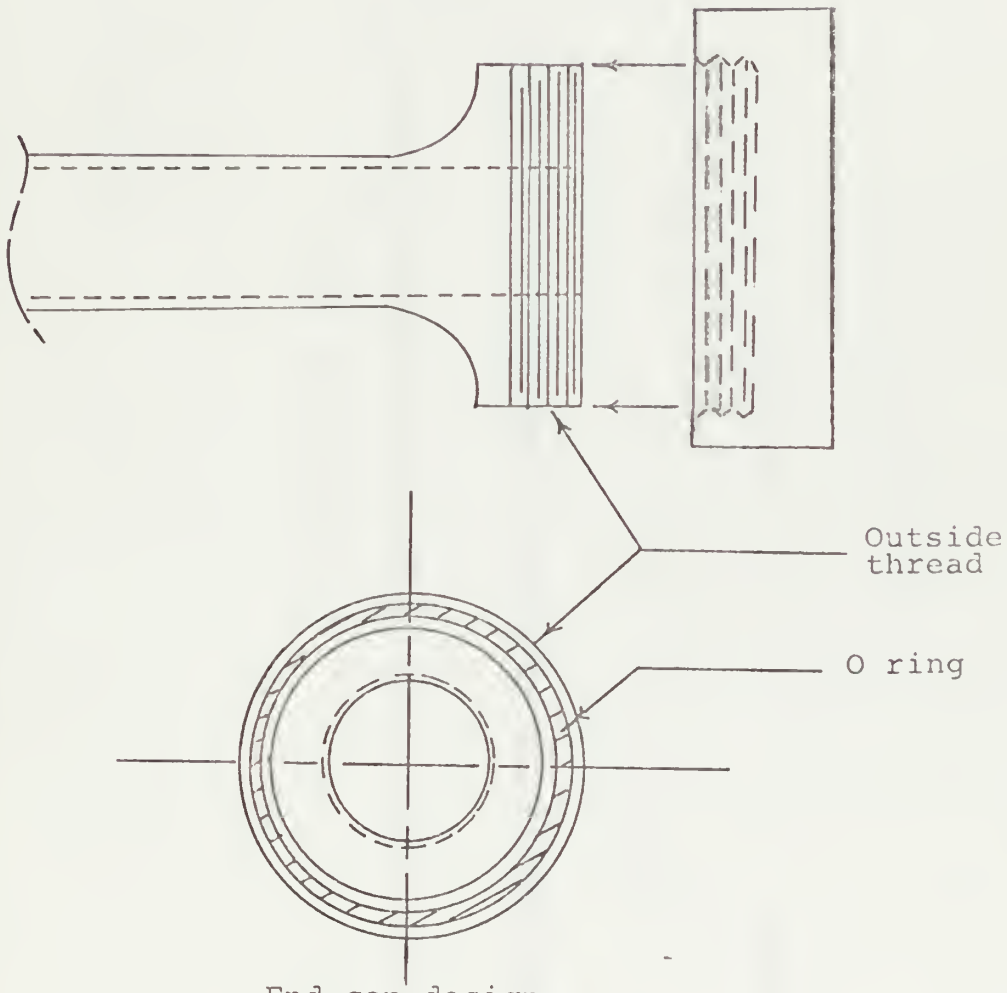

End cap design
figure 3

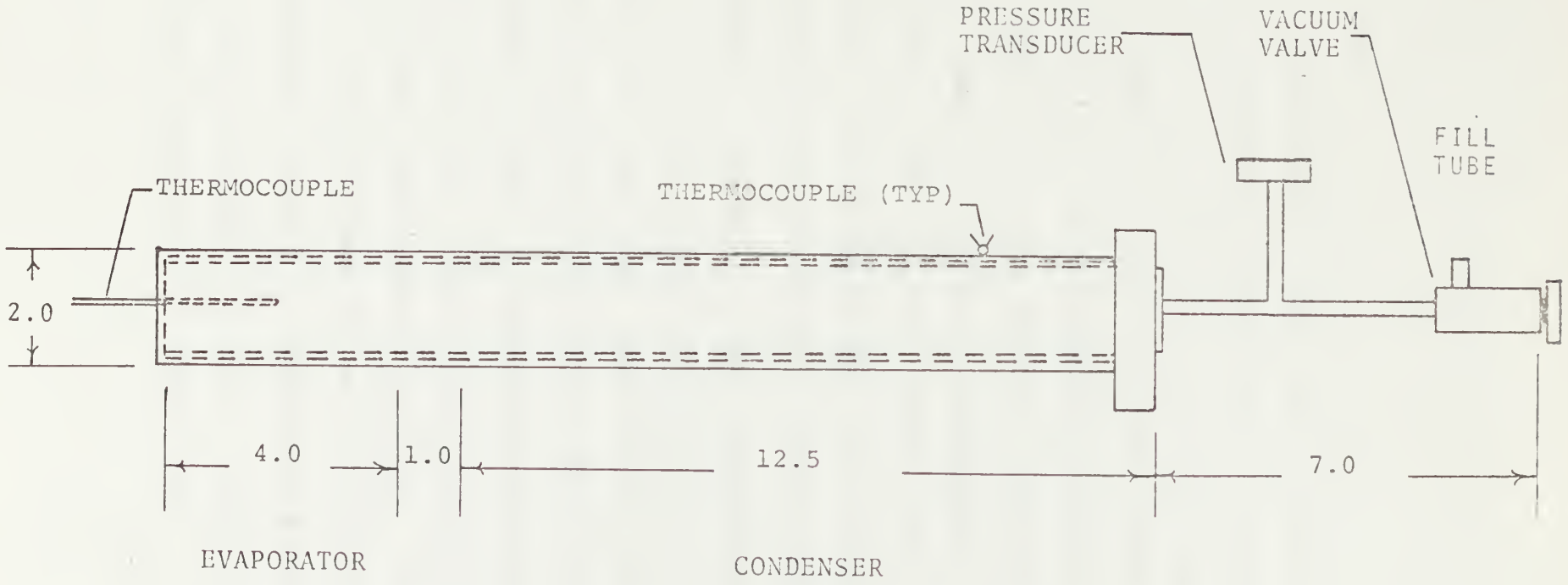

Overall heat pipe design
figure 4

B. DESIGN CONSIDERATIONS

The performance of a heat pipe is affected by any chemical reaction or decomposition of the working fluid or the corrosion or erosion of the wick, spring, or heat pipe. An example is the reaction of water and stainless steel resulting in the release of hydrogen gas. In designing a heat pipe the materials used for the pipe and the wick must be chosen to be compatible with each other and the working fluid. For this reason, the screen mesh, pipe and spring wire were all made of the same material, stainless steel.

Because the heat pipe operation is dependent on capillary pumping the working fluids surface tension had to be considered. In addition, the gravitational force and flow losses made the consideration of the working fluid's density and viscosity important. Methanol, whose properties are slightly less desirable than water was chosen because of its good wetting characteristic and high compatibility with stainless steel. Ammonia was rejected because of its toxicity.

Following Marcus [Ref. 7], the screen mesh size and dimensions of the pipe for a given working fluid can be related by a pressure force balance equation. This equation is based on the principle that the net capillary head in the wick must be greater than the losses due to pressure drop in the vapor and liquid plus any losses due to body forces. This force balance equation is expressed as:

net capillary head	-	body force head	$\geq$	liquid pressure drop	-	vapor pressure drop

$$\Delta P_c - \Delta P_b \geq P_L + \Delta P_v$$

where, $\Delta P_c = \frac{4\sigma}{\delta}$

$$\Delta P_b = 2R_w \rho_L$$

$$\Delta P_L = \frac{L \mu_L \dot{m}_L}{2\pi J \rho_L (R_w^2 - R_v^2)}$$

and $\dot{m}_L = \frac{Q}{h_{fg}}$

and the vapor side pressure drop is assumed to be much less than the other pressure components and therefore not considered.

The heat load was anticipated to be in the range of zero to 100 watts with the most probable loading between 10 and 50 watts. The stainless steel screen mesh was available in various sizes up to 200 wires per inch. Using this information and the above force balance equation an iterative design ensued for an operating temperature of 120 to 170 °F. Various screen wire spacings, lengths of pipe and number of layers of mesh were combined with various pipe diameters in seeking the proper design. The design centered on providing for a pipe from one to two feet long and with a diameter in excess of one inch if possible.

With a margin of safety, the design was tentatively set for a two-inch diameter pipe of overall length 15 inches with 5 layers of 150 mesh screen. This length allowed for a 4 inch heater section and a one inch adiabatic section. This was the tentative design because these parameters were for a heat pipe not loaded with a non-condensable gas. To achieve an optimum design for the gas loaded heat pipe the design program developed by Marcus [Ref. 7] was employed.

In order to use this program the non-condensable gas had to be selected. The choice centered around the inert gases since they were chemically inactive and provided a good spectrum of molecular weights. To assist in emphasizing the effect of gravity on the vapor-gas mixture a large difference in the molecular weights of the working fluid and the non-condensable gas was needed. The choice of krypton allowed a molecular weight ratio of krypton to methanol of approximately 2.5.

With the heat pipe parameters tentatively determined, Marcus' computer program was used to first determine the additional length of pipe needed for the non-condensable gas and then to give a performance prediction. Two inches were added to the condenser to allow for the proper performance of the heat pipe with the non-condensable gas. A check of the preceding force balance equation used in the design process indicated the heat pipe would still operate satisfactorily with the extra 2 inches of length.

C. INSTRUMENTATION

The instrumentation of the heat pipe included both temperature and pressure sensors. Seventeen thermocouples were placed in line in the grooves of the fins at an interval of approximately 0.650 inches on the top of the pipe. An additional thermocouple was placed inside the pipe. This thermocouple, enclosed in a stainless steel sheath, was inserted 2 inches through the evaporator end plate. The condenser thermocouples were 0.010 inches in diameter copper and constantan wires welded with a bead at the end. The bead was made with a Dynatch thermocouple welder. These beads were attached to the grooves of the condenser with a Unitek model 1065 welder. The other end of all the thermocouple wires were led to a Jones strip and from there to a Hewlett Packard 2010C Data Acquisition System.

Several layers of Johns Manville MinK insulation were wrapped around the heater to minimize heat losses. Two additional thermocouples were then placed across a layer of insulation. By knowing the temperature difference across a layer of insulation as well as the thermal conductivity and thickness of the insulation the heat loss from the evaporator could be estimated.

To determine the power input to the heater accurately a known resistance was placed in series with the Nichrome heater strip. By measuring the voltage across the known resistor the heater current was determined. This current was used with the voltage reading across the heater to

determine the power input at the evaporator section. A Hewlett Packard digital voltmeter was used for these measurements.

The pressure was measured by a Pace KP-15 transducer and recorded on a Hewlett Packard 7702B recorder. Figure 5 shows a schematic diagram of the heat pipe and its associated equipment. Included in this diagram and in Figure 6 is the apparatus used to fill the heat pipe with the required amount of methanol and non-condensable gas. The filling rig used was a previously existing device used by J. Woodard [Ref. 8] which was modified to include an inlet for the non-condensable gas and an additional vacuum valve.

D. CALIBRATION AND ERROR ANALYSIS

The thermocouples were calibrated in a constant temperature bath with a platinum wire resistance thermometer and a Rosemont commutating bridge, while the thermocouple readings were made on a Leeds and Northrop K-3 precision potentiometer. The thermocouple readings were found to vary from the commutating bridge temperature readings by no more than $\pm 0.11°F$. The data acquisition system was then checked against the Leeds and Northrop potentiometer and found to have an error bound of $\pm$ 0.4°F. The resistor placed in series with the evaporator heater was also calibrated on the Rosemont commutating bridge. The resistance was read as 2.013 $\pm$ 0.0002 ohms. The Harrison pressure recorder and Pace transducer were calibrated with a Wallace and Tiernan gauge. The error for the transducer and recorder was $\pm$ 0.4 psia.

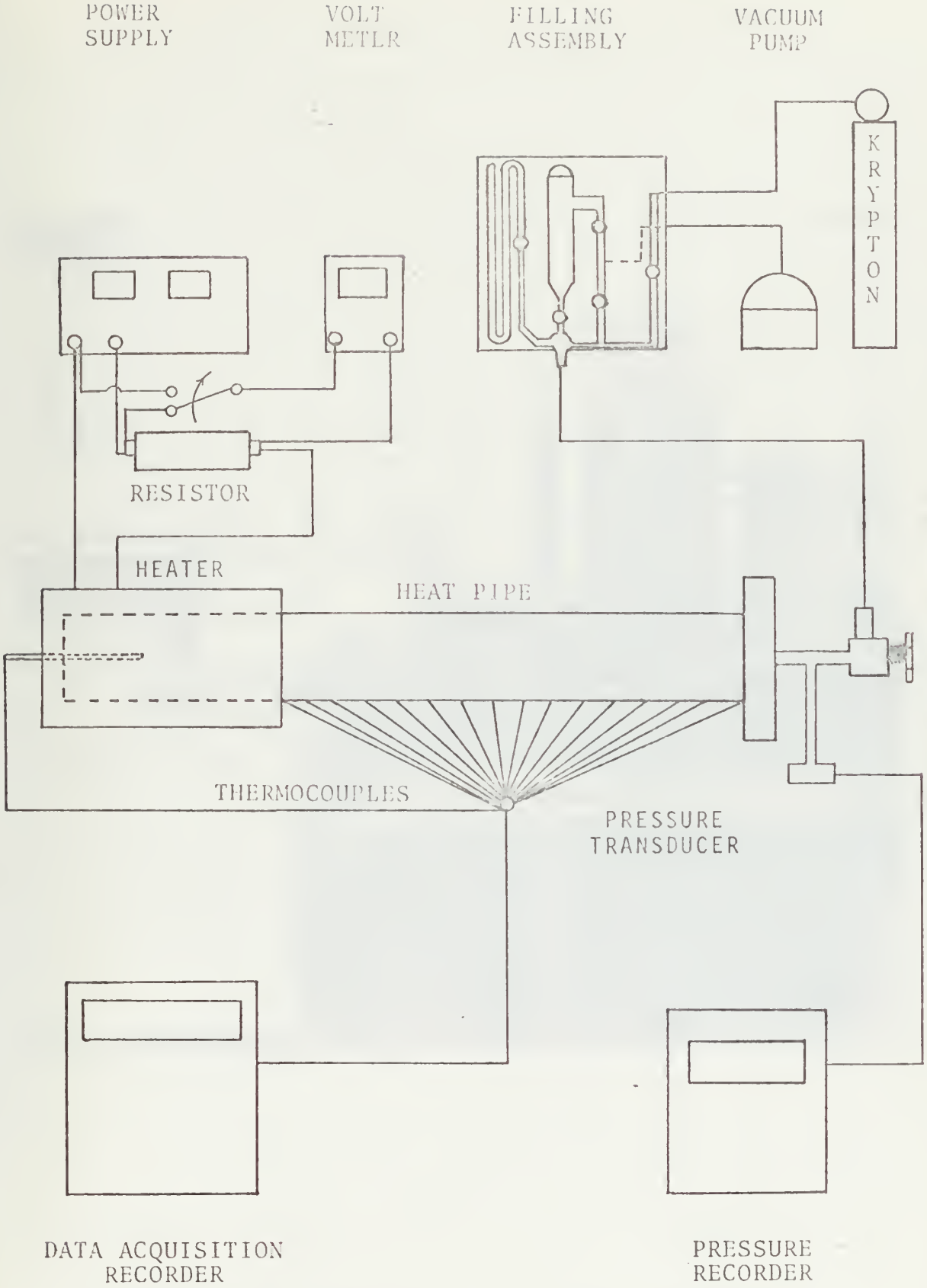

Diagram of heat pipe and associated equipment
figure 5

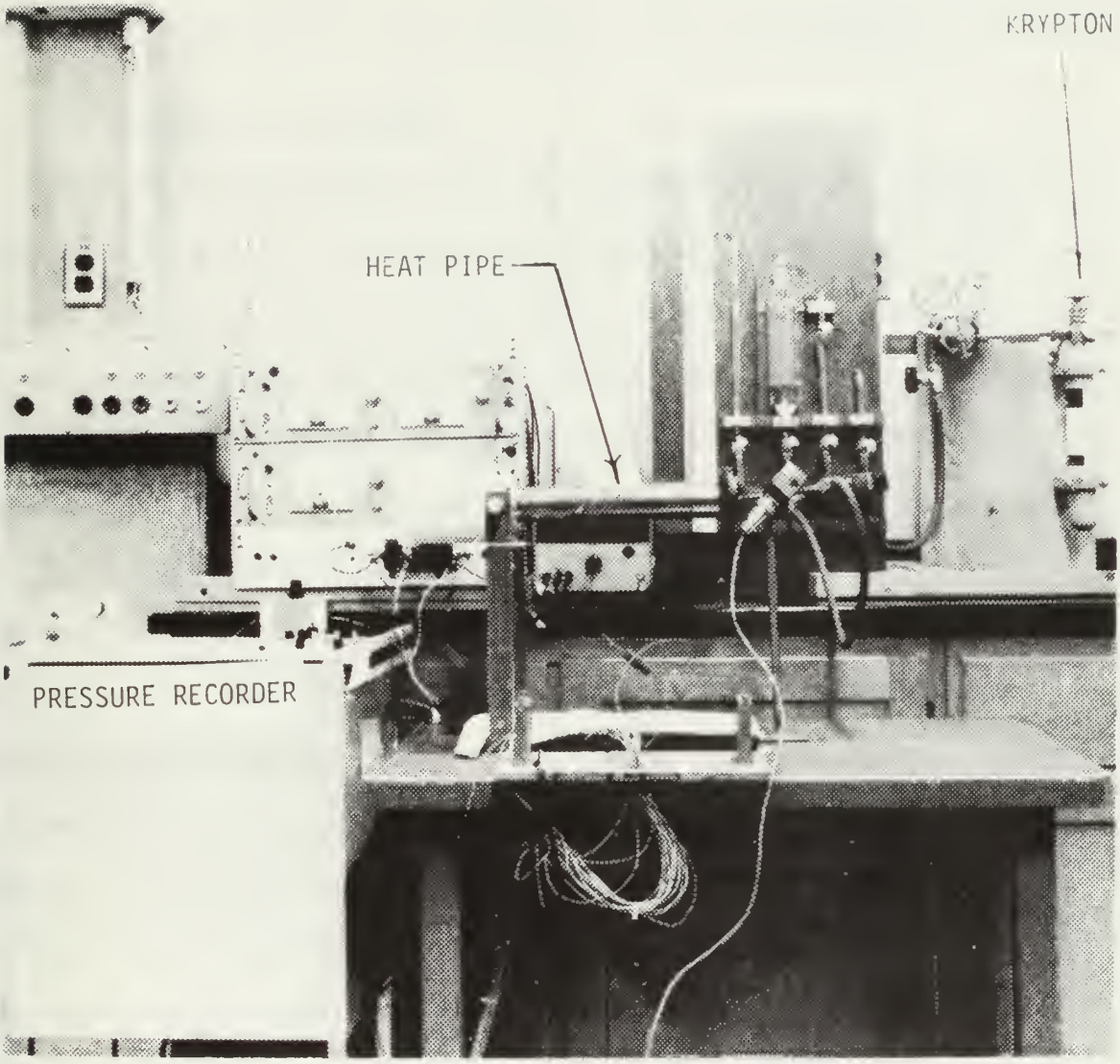

Photograph of heat pipe and associated equipment
figure 6

An error analysis was performed for all the data recorded as well as the other parameters used in computations. A summary of the error bounds is shown in Appendix A along with sample calculations. The data points on the graphs were drawn to include the error bounds of the information presented.

E. EXPERIMENTAL PROCEDURE

Prior to proceeding with the experiment, the amount of working fluid to be used was determined. The equivalent liquid volume of the working vapor for a heat input of 50 watts was added to the void volume of the wick structure. The volume of methanol required was approximately 45 milliliters depending on the safety factor used. Operation of the heat pipe with 30, 40, and finally 55 milliliters of methanol produced no discernible difference in the temperature and pressure readings. Since wick dry out, caused by a shortage of working fluid in the wick structure, can cause a breakdown in the capillary pumping process the choice was made to use 55 milliliters of methanol. An excess of working fluid would not produce any detrimental effects on the heat pipe's performance. The krypton gas used in the experiment was research grade while the methanol working fluid was spectrophotometric quality.

Prior to assembling the heat pipe, the pipe, wick, end cap, and spring were all scrubbed with acetone and rinsed three times with distilled water. The assembled heat pipe was subjected to the same process prior to attaching the end plate. The procedure used in preparing the assembled heat

pipe for operation started with evacuation of the heat pipe and filling assembly. The filling assembly, in addition to supplying the working fluid and non-condensable gas, provided for the connection of the heat pipe to the evacuation pump. A total of approximately 30 inches of 0.25 inch inside diameter vacuum hose connected the heat pipe through the filling assembly to the evacuation pump. The pump was able to achieve vacuum, read at the pump, of 2×10^{-6} millimeters of mercury.

When the evacuation was completed the heat pipe and filling assembly were isolated from the evacuation pump. A measured amount of methanol was then released into the heat pipe. The pressure was recorded when the temperature inside the pipe equalled ambient temperature . The krypton was next released from its high pressure cylinder and allowed to flow into the heat pipe, while monitoring the pressure and internal temperature. The amount of krypton present could then be calculated by using the temperature and the difference between the pressure reading and the partial pressure of methanol with the perfect gas equation. When the internal temperature of the pipe was equal to the ambient temperature, it was recorded along with the pressure in the heat pipe.

The heat pipe was then isolated from the filling assembly by means of the vacuum valve on the stem of the heat pipe's end cap. The pipe was then positioned for the desired angle of operation and the heat input was applied.

The temperature and pressure readings were monitored until a steady state operation was detected. The steady state condition was based on the condenser temperatures rate of change being less than 0.5 °F per hour.

The temperatures and pressure were recorded at steady state, then the heat pipe was either repositioned or the heat input was altered to initiate a new operating mode. This process was continued until sufficient data had been obtained.

Shutdown of the pipe required only the removal of the heat input and subsequent release of the internal fluids when the heat pipe had achieved ambient temperature.

III. EXPERIMENTAL RESULTS

A. CONVENTIONAL HEAT PIPE

The heat pipe was initially operated as a conventional heat pipe with only methanol present. Heat inputs were applied from 10 to 50 watts in 10 watt increments in each of three heat pipe positions; horizontal, condenser raised 45°, and vertical. The data presented in Figures 7, 8, and 9 is representative of all the condenser temperature readings for the various heat inputs and positions mentioned. As these Figures show, the entire condenser operated in an isothermal manner as expected.

Figures 10 and 11 show the evaporator temperature and condenser pressure for a particular heat input. The data points so obtained for each of the heat pipe positions are connected with smooth curves. The evaporator temperatures were used to determine the saturated vapor pressure of methanol from the data on methanol presented by J.M. Smith [Ref. 9]. The pressures obtained from J. M. Smith's table were all within ± 5% of the corresponding pressure readings of Figure 10. Therefore, the assumption of operation of the heat pipe with a saturated working vapor is confirmed. The temperature readings used to enter J. M. Smith's table were from the evaporator while the pressure reading used for comparison were taken from the end of the condenser. The fact that the pressures are equivalent, within the

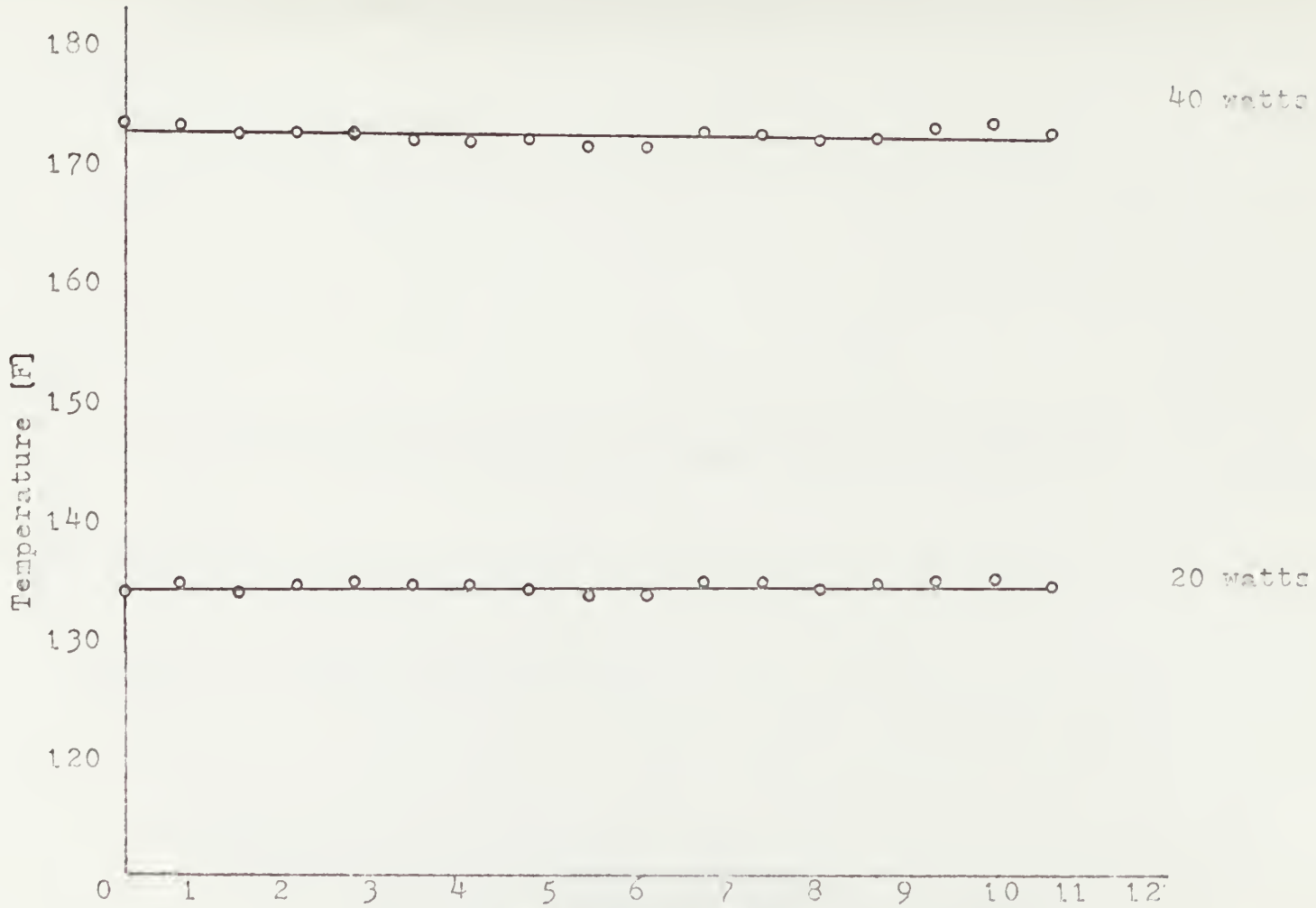

Horizontal position, condenser temperature, methanol
figure 7

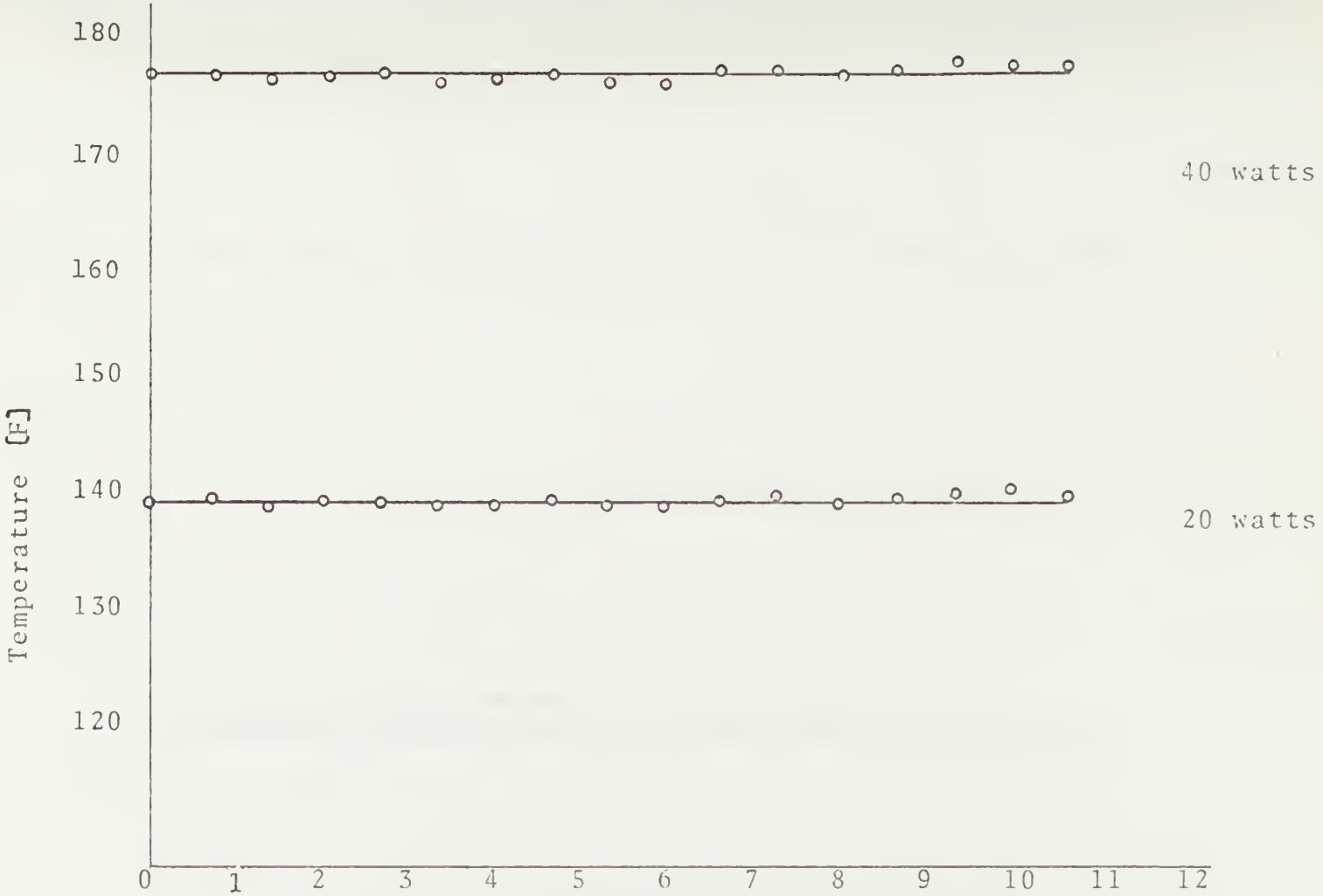

45 position, condenser temperature, methanol
figure 8

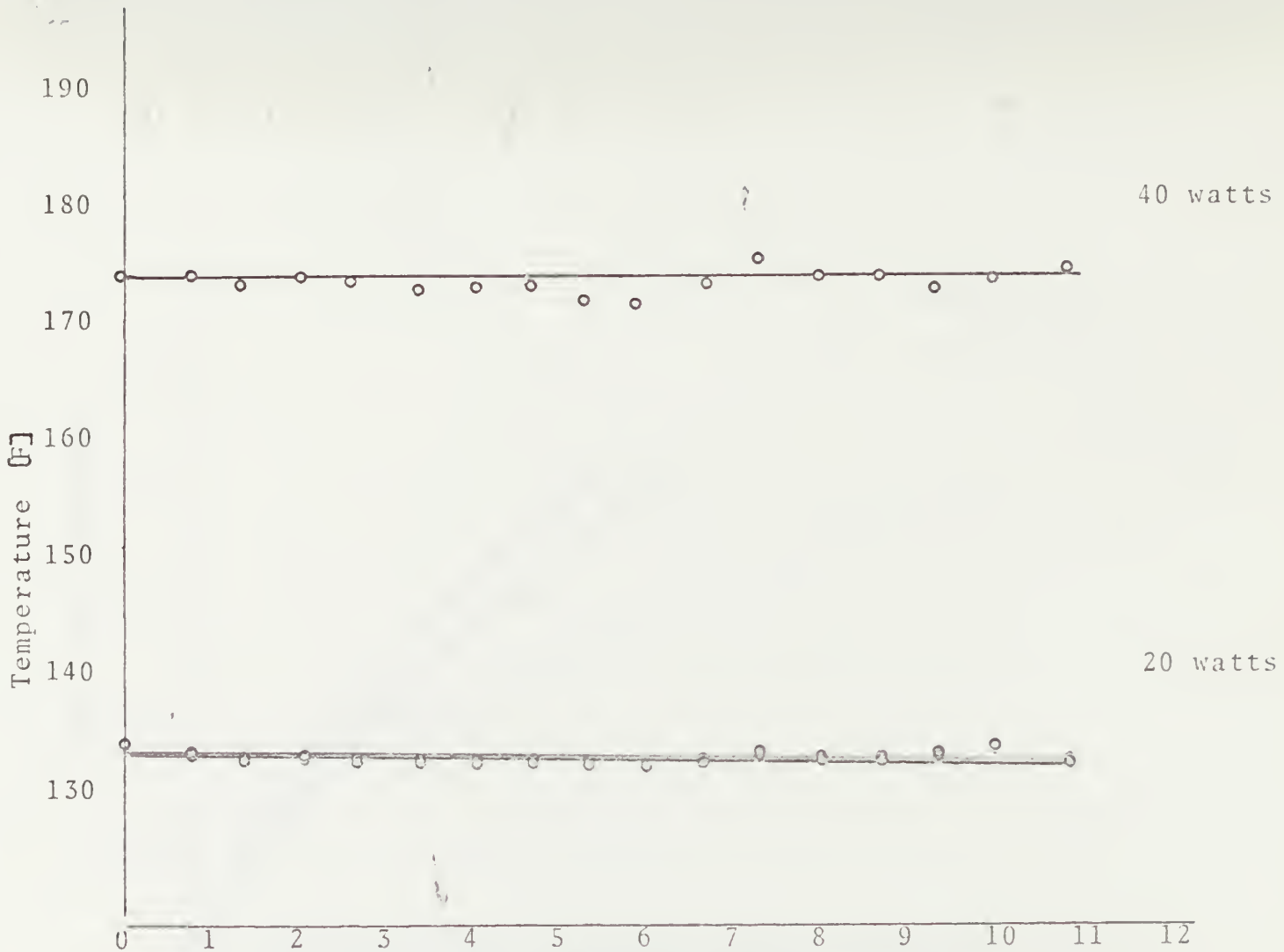

Vertical position, condenser temperature, methanol
figure 9

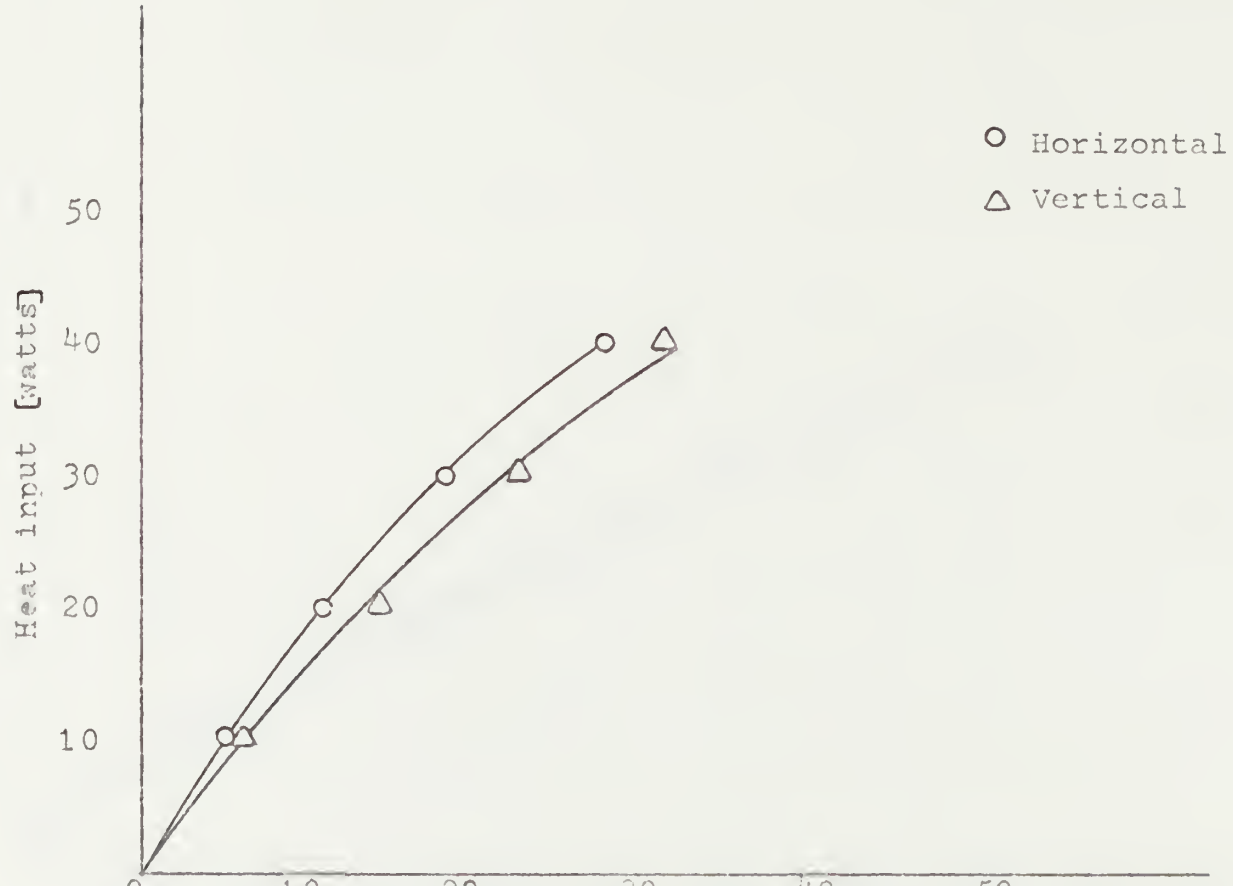

Heat input-condenser pressure, methanol

Figure 10

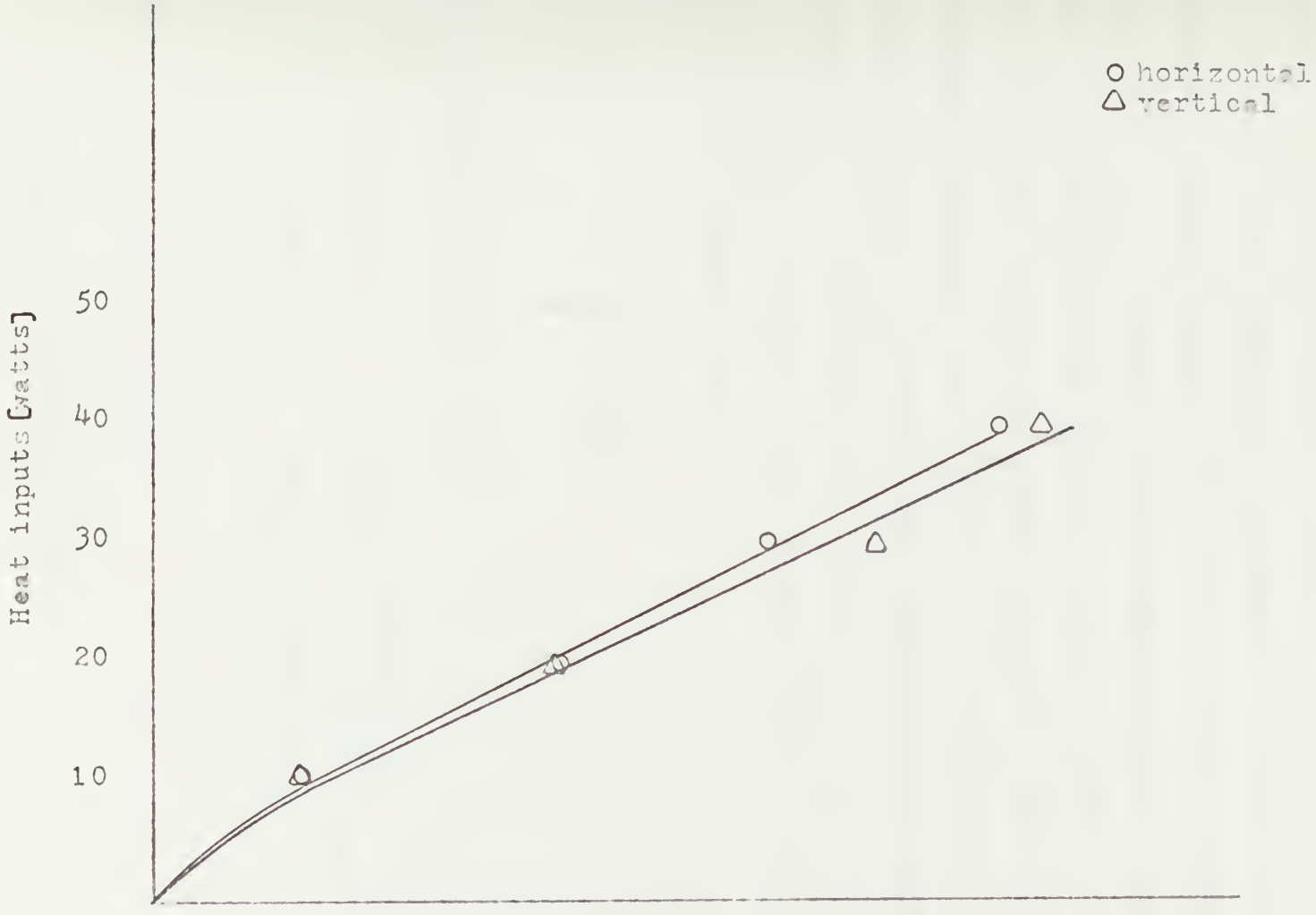

Heat input-[illegible] for [illegible], vertical

Figure 11

accuracy of this experiment, and were read at opposite ends of the pipe indicates that there is no pressure gradient throughout the conventional heat pipe during operation.

Figure 11 indicates the heat input to the heat pipe as a function of the evaporator temperature for the horizontal and vertical positions. The variation of the evaporator temperature for the changes in heat input is shown to be linear. The slope for the vertical position in Figure 11 is less than that for the horizontal position. This indicates higher evaporator temperatures for the same heat input in the vertical position when compared to the horizontal position. An explanation for this can be found in the heat transfer coefficient of the cylinder which is directly related to the Nusselt Number by:

$$h = \frac{N_{NUL}\ k}{L}$$

where the Nusselt Number equals:

horizontal $\qquad N_{NUL} = .525(N_{Pr}\ N_{Gr})^{.25}$

vertical $\qquad N_{NUL} = .59(N_{Pr}\ N_{Gr})^{.25}$

where:

$$N_{Gr}N_{Pr} = \frac{L^3\ \rho^2\ g\ \beta\ \Delta T\ C_p}{\mu\ k}$$

where L is the significant length and equals:

the pipe diameter for the horizontal position,
the overall pipe length for the vertical position.

Since the overall length of the heat pipe is approximately 9 times its diameter the heat transfer coefficient for the horizontal pipe exceeds that for the vertical case. For the same heat input the decreased heat transfer coefficient in the vertical position, when compared to the horizontal position, requires a greater temperature difference between the heat pipe and the atmosphere. This is reflected in Figure 11.

B. GAS LOADED HEAT PIPE

After evacuation the heat pipe was filled again with 55 milliliters of methanol and 2.5×10^{-3} poundmass of krypton gas. The heat pipe was operated over a similar range of heat inputs and the same three positions. The condenser temperature profile for various heat inputs and positions are shown in Figures 12, 13 and 14.

Figures 12 and 13 representing the horizontal and 45° position, show only a nomial negative temperature slope from the evaporator end of the condenser. This temperature profile indicated the concentration of working vapor was decreasing very little in the direction of decreasing temperature. It was anticipated that a larger temperature gradient would be present, reflecting a more marked

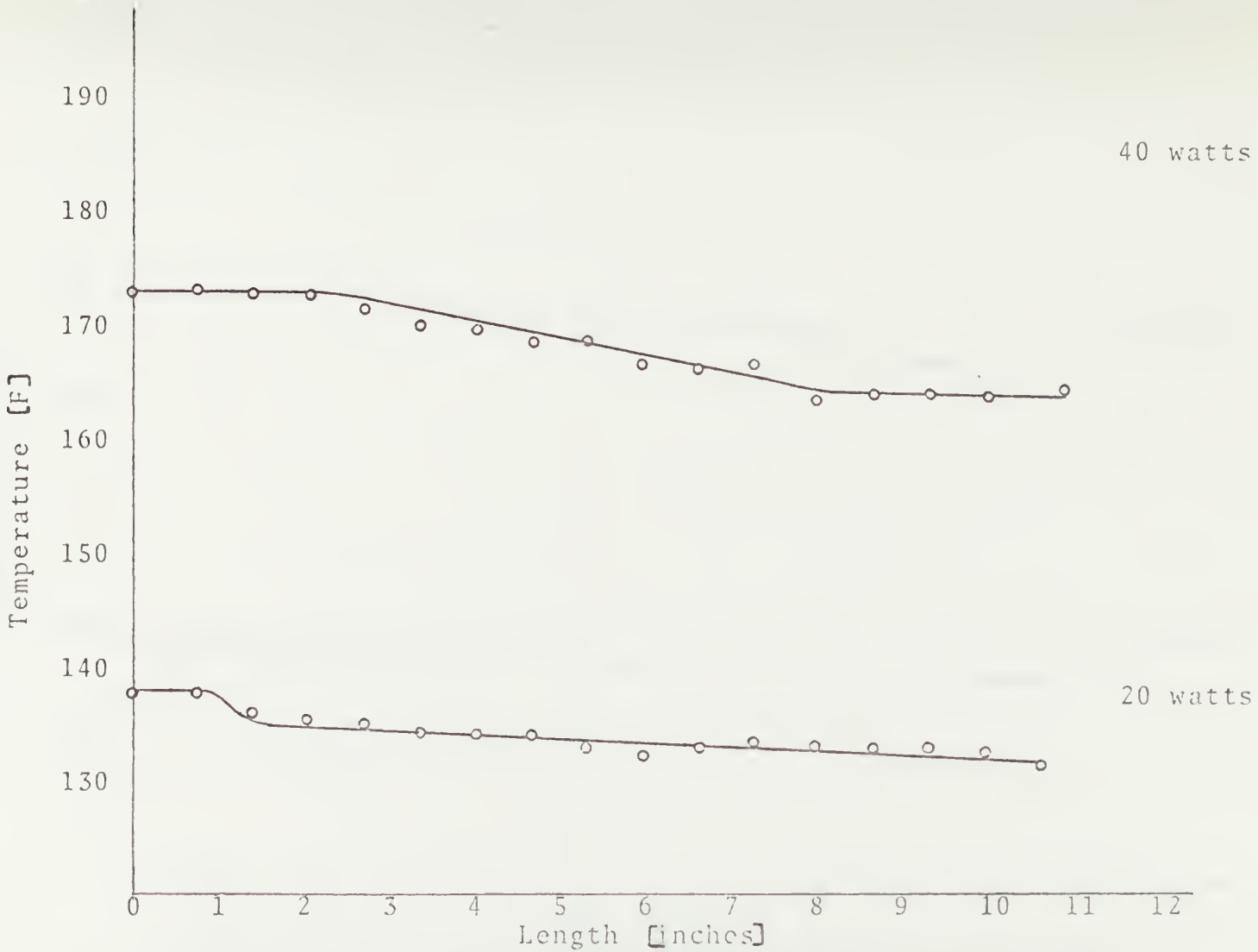

Horizontal position, condenser temperature, methanol and krypton
figure 12

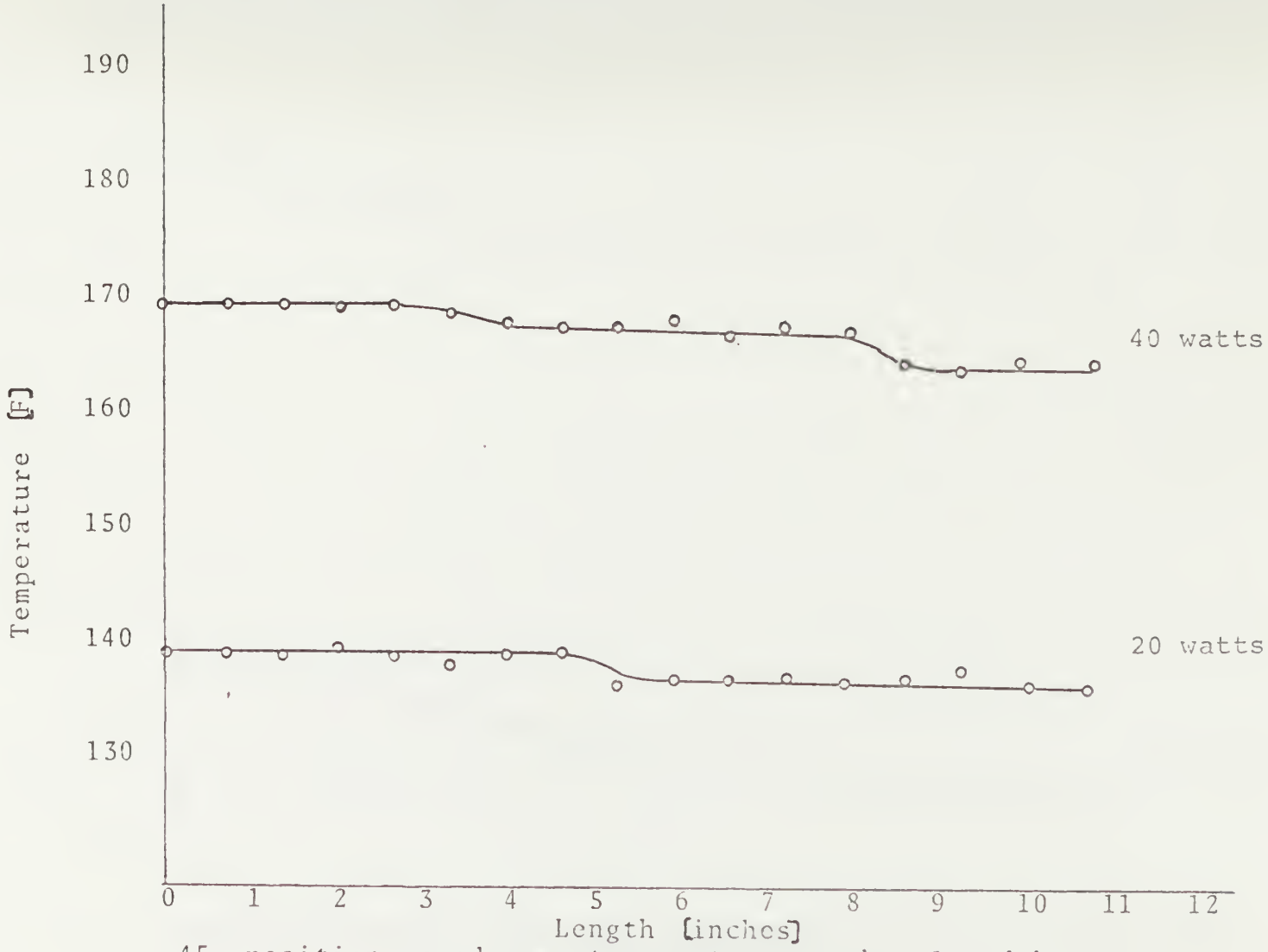

45 position, condenser temperature, methanol and krypton
figure 13

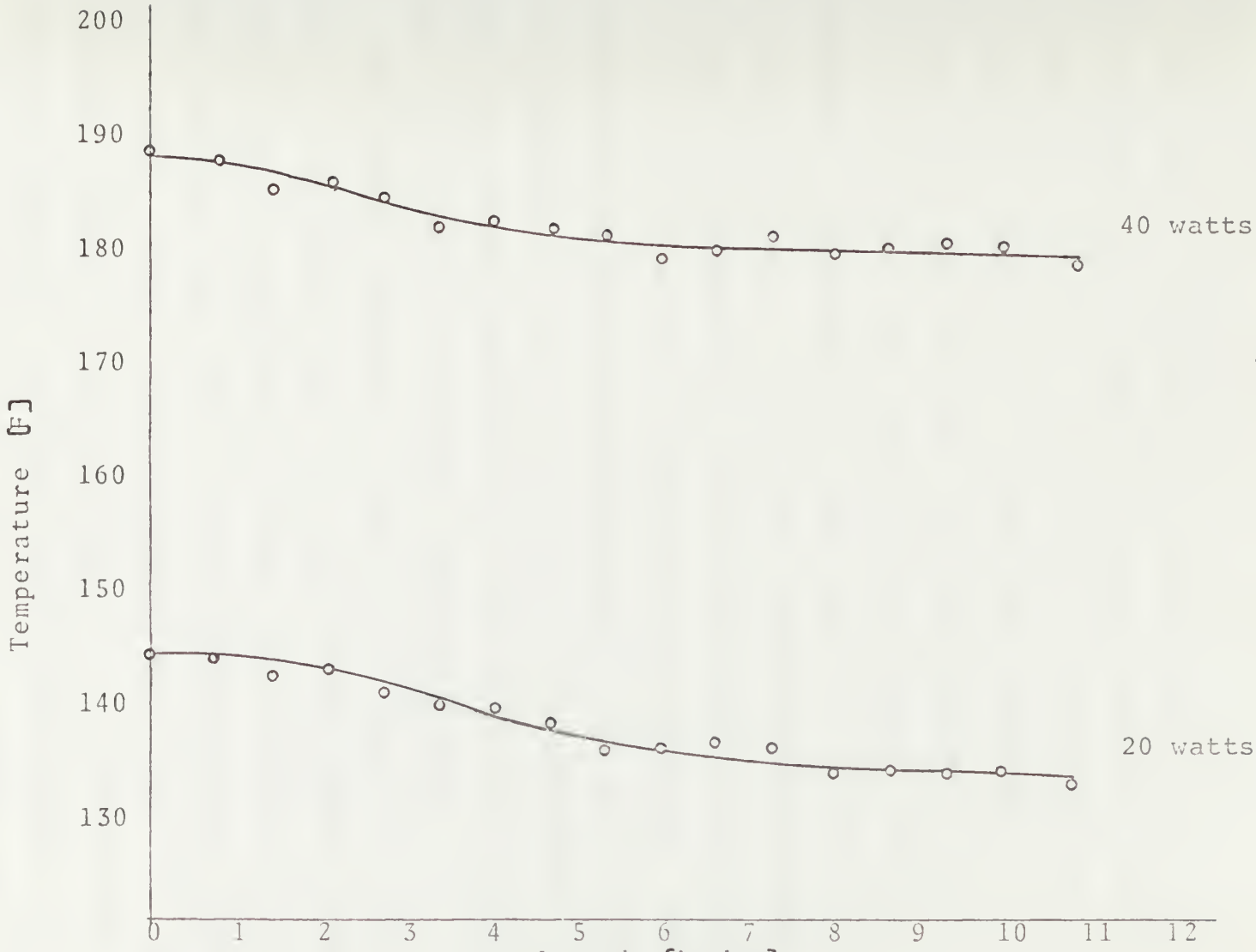

Vertical position, condenser temperature, methanol and krypton
figure 14

segregation of the working vapor and the gas. It was further anticipated that this front between the vapor and gas would spread out over more of the condenser as the angle of the heat pipe increased.

The vertical operating position, as shown in Figure 14 had a larger negative temperature slope than that found in the other two positions. The vertical position appears to indicate the absence of a sharp front but rather a mixture of the vapor and gas. The concentration of the vapor does decrease more markedly with distance from the evaporator in this position. This indicates that inspite of the gravitational force and the larger molecular weight of the non-condensable gas, the gas does tend to accumulate in the condenser at the end away from the evaporator. The concentration of the non-condensable gas at no point excludes the condensation of the working fluid in the condenser. Therefore, the gravitational force does effect the variable conductance property of the gas loaded heat pipe.

In comparing Figures 7, 8, and 9 with Figures 12, 13 and 14 it is apparent that the change in temperature of the condenser for a variation in the heat load was less for the gas loaded heat pipe. This is also indicated by the larger slope found in Figure 11 when compared with Figure 16. This is another feature of the gas loaded heat pipe due to its variable conductance. As these two figures indicate, the operating temperature of the evaporator is higher, for the same heat input, for the gas loaded heat pipe. Figures 10

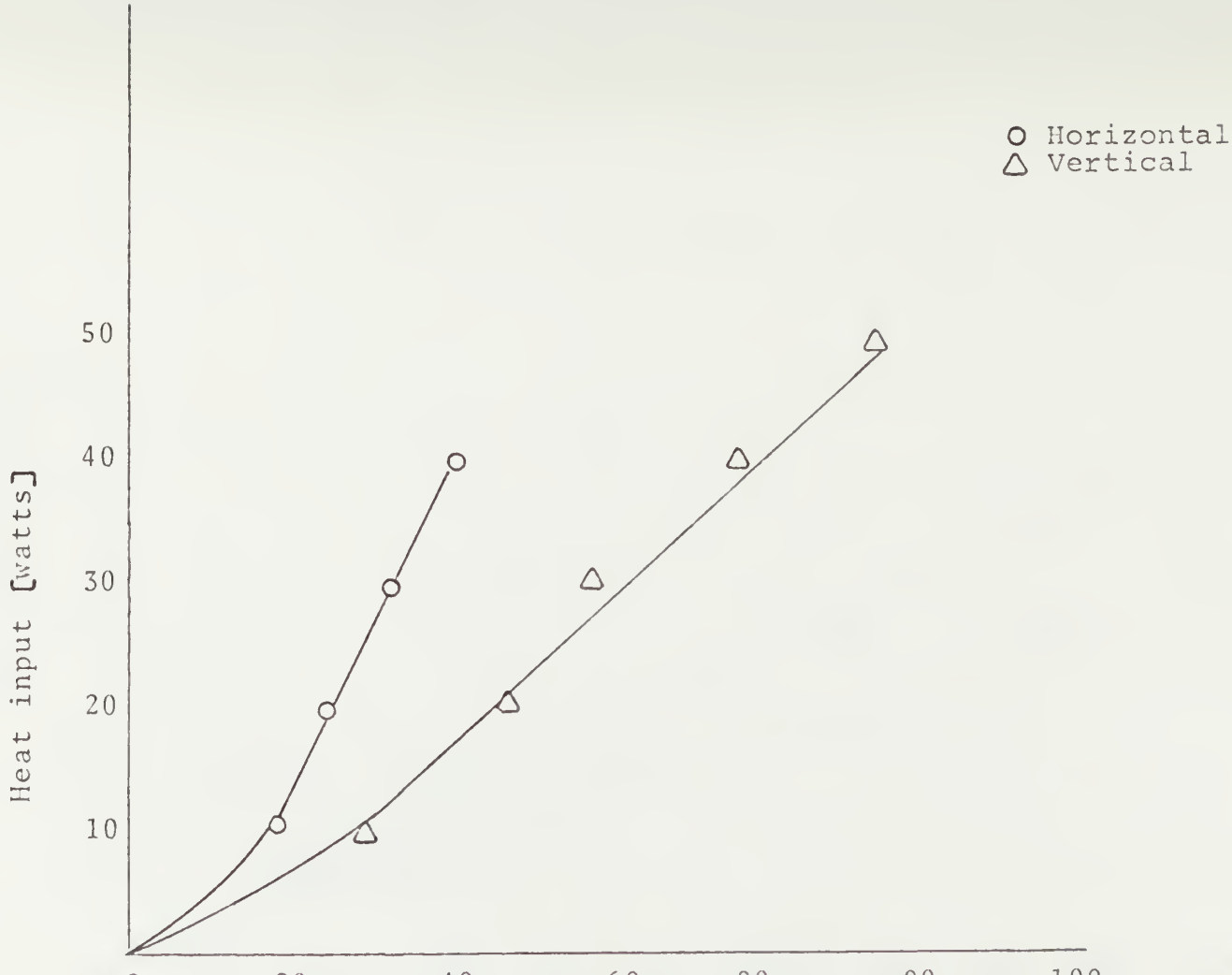

Heat input-condenser pressure, methanol and krypton
figure 15

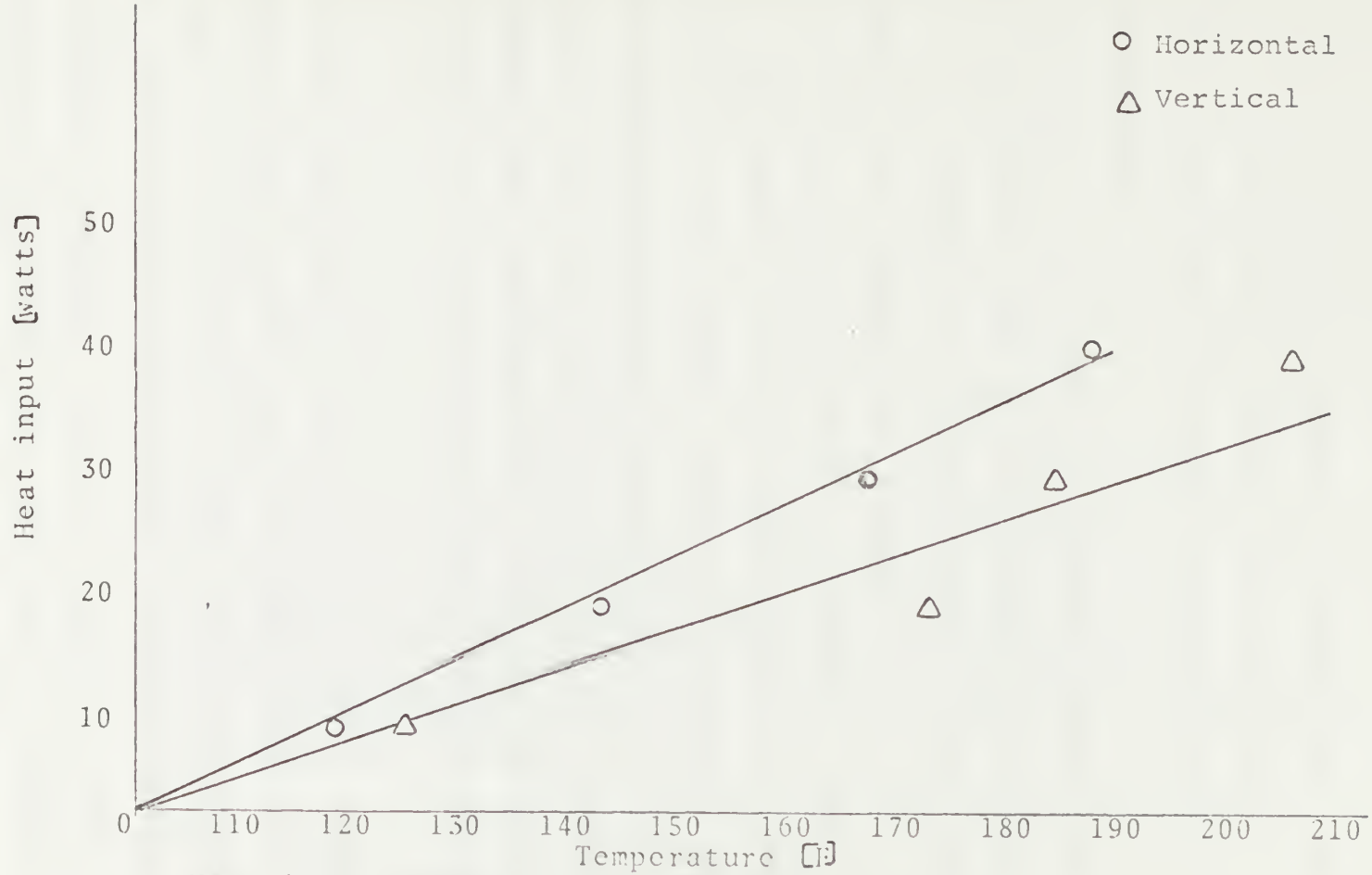

Heat input-evaporator temperature, methanol and krypton
figure 16

and 15 indicate that, as expected, the pressure is greater in the gas loaded heat pipe compared to the conventional heat pipe for the same heat input.

The lack of a significant temperature variation in the condenser for the horizontal position was investigated further after the data had been collected for all heat inputs and positions.

The heat pipe, in the horizontal position was rotated around its longitudinal axis in order to allow the thermocouples to take readings along the bottom of the heat pipe. In this position the readings were uniform and on the average 12 °F lower than those taken on the top of the heat pipe. The bottom of the pipe was expected to be cooler than the top due to the natural convection. However, the temperature slope on the top of the pipe and the absence of such a slope on the bottom indicated that the non-condensable gas and methanol may have stratified. That is, the krypton may have settled on the bottom of the entire length of the pipe.

If the gas vapor had not stratified the nominal temperature gradient present on the top of the pipe would have been present on the bottom of the pipe. With stratification, the heavier krypton would settle to the bottom portion of the horizontal condenser. This would greatly reduce the condensation rate if not completely stop it in this section. The bottom of the heat pipe being greater than

ambient temperature can be accounted for by the circumferential conduction of the pipe.

To further investigate this, temperature sensitive liquid crystals were applied over a 2 inch wide black paint strip which had been applied to the entire length of one side of the condenser. The liquid crystal has the characteristic of changing from clear to a color over a small temperature range. The crystals used were R53. These indicated three distinct temperature ranges by three different colors as indicated below [Ref. 10]:

Color	Temperature °C
Red	50.5 ± 0.5
Green	52.1 ± 0.5
Blue	53.3 ± 0.5

With the liquid crystals on the pipe the heat input was varied until the general temperature range for crystal coloring was achieved. Figure 17 shows two photographs of the isotherms observed for the indicated power input. In the case of a heat pipe the isotherm represents a line of constant working vapor density. The fact that the isotherm lines run down the side of the pipe in a near horizontal manner indicates the working vapor density varies in the same manner. Stratification to some degree may therefore be present.

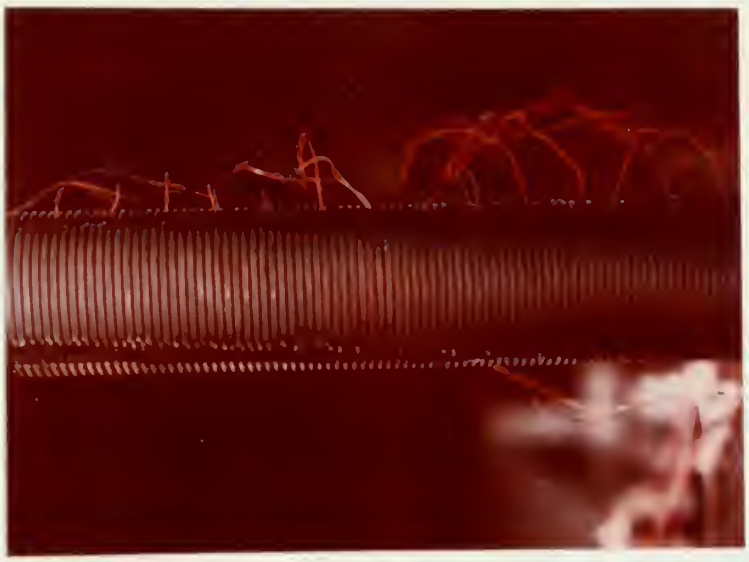

Heat input equals 21.70 watts

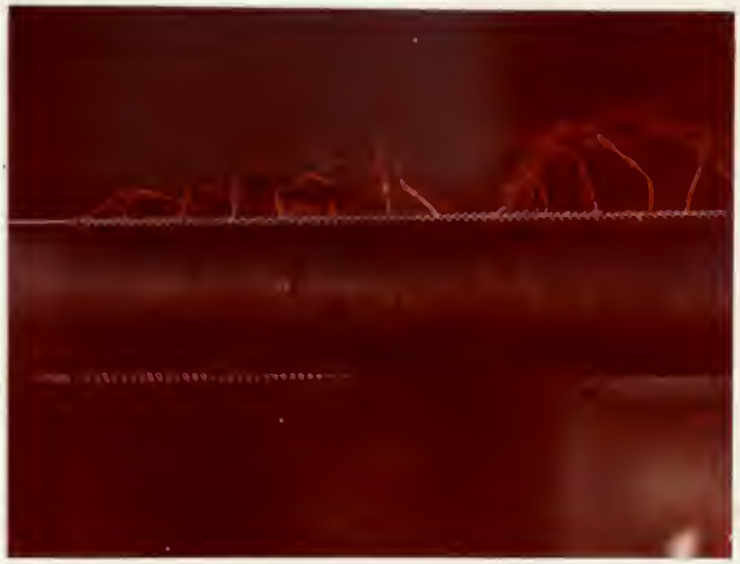

Heat input equals 23.6 watts

Photographs of liquid crystals on condenser
figure 17

The effect of natural convection upon the slope of the isotherms has not been fully investigated at this time and would provide more insight into this phenomenon. The implications of the possibility of stratification will be discussed in Section V.

IV. ANALYSIS

A. THEORY

The analysis developed in this section is for the condenser section of a gas loaded heat pipe. The development is through the application of the continuity and momentum equations for one dimensional flow, the energy equation for the wall, wick, and fin heat transfer as well as Fick's law of diffusion and the perfect gas law. The development resulted in four first order differential equations which were solved simultaneously with the use of a Runge Kutta routine. The formulation of this analysis is outlined below. It should be noted that as Figure 18 indicates, the origin of the coordinate system is at the end of the pipe away from the evaporator.

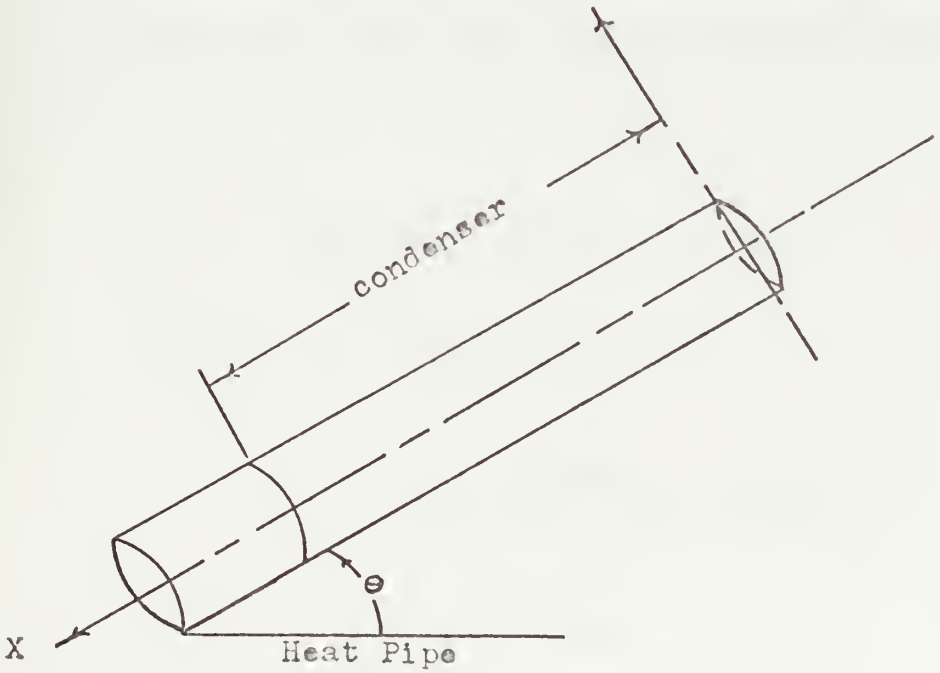

figure 18

Starting with the integral form of the momentum equation as applied to the section shown in Figure 19:

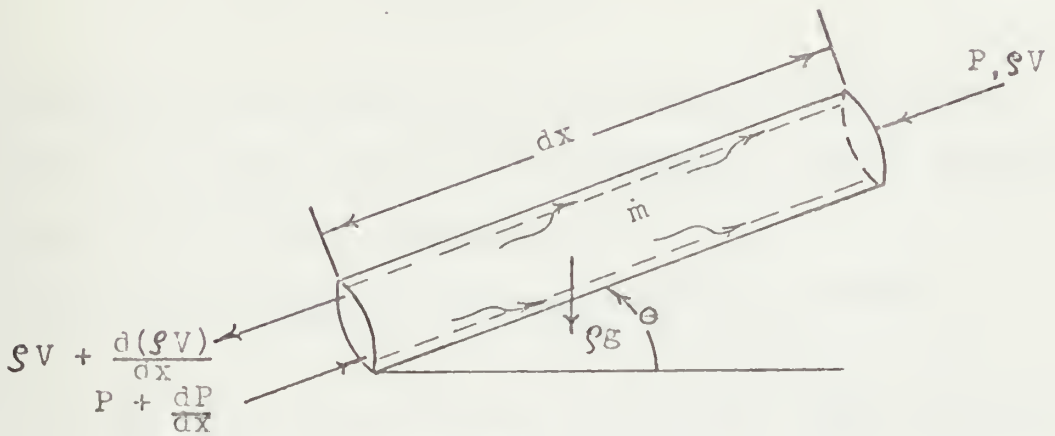

figure 19

$$(1) \qquad \sum F_x = \int \rho V(V \cdot dA_c)$$

In the following analysis the viscous term has been left out of the above equation. This simplifying assumption is based on the Reynolds number being very small in the operating range of the heat pipe. For a typical heat load of 20 watts:

$$R_D = \frac{V\,D}{\nu} = 50.0$$

where, $$V = \frac{Q}{h_{fg}\, A_c\, \rho}$$

$$V = \frac{68.26}{(481)\ \frac{\pi}{4}\ (1/6)^2\ (1/20)}$$

$$V = .04 \text{ ft/sec}$$

For fully developed laminar flow the friction factor f can be represented by $64/R_D$. This results in a shear force:

$$F = 8\mu\pi V\, dx$$

Considering the entire one foot length of condenser the force is in the range of 10^{-6} pounds or less. Therefore, the shear force can be neglected.

Referring to Figure (19), equation (1) becomes:

$$P - [P + \frac{dP}{dx} dx] + \rho g \sin\theta\, dx = -\rho V^2 + [\rho V + \frac{d}{dx}(\rho V)\, dx]$$

$$[V + \frac{dV}{dx} dx] + \dot{m}\, V_a\, \pi\, D\, dx$$

where P is the pressure in the condenser section, V is the vapor-gas velocity, V_a is the velocity of the vapor, ρ is the vapor-gas density, g is the gravitational acceleration and D is the diameter of the vapor space.

Dividing by $A_c dx$, and taking the limit as dx approaches zero gives:

$$(2) \quad -\frac{dP}{dx} + \rho g \sin\theta = \rho V \frac{dV}{dx} + V \frac{d(\rho V)}{dx} + \dot{m}\, V_a \frac{\pi D}{A_c}$$

The continuity equation for the mixture is:

$$\rho V A_c = \dot{m}\, \pi\, D\, dx + [\rho V + \frac{d}{dx}(\rho V)\, dx]\, A_c$$

or

$$(3) \qquad \dot{m} \frac{\pi D}{A_c} + \frac{d}{dx}(\rho V) = 0$$

Applying Fick's First Law to species a:

$$\rho_a V_a = \rho_a V - \rho \mathfrak{D} \frac{dw}{dx} \tag{4}$$

where $\mathfrak{D}$ is the diffusion coefficient for the vapor-gas mixture, ρ_a is the density of the vapor and w is ρ_a/ρ.

An alternate form of this equation is:

$$V(w - 1) = \mathfrak{D} \frac{dw}{dx} \tag{5}$$

The pressure in the heat pipe condenser, P, is the sum of the partial pressure of the vapor, P_a, and the partial pressure of the gas, P_b:

$$P = P_a + P_b$$

The perfect gas law can be used for the non-condensable gas. This is possible because the operating temperature and pressure in the heat pipe are well below the critical point of the gas. However, during heat pipe operation the working fluid vapor is in a saturated state which precludes use of the perfect gas equation. Instead the pressure of the working fluid vapor can be represented as a function of temperature only. Therefore,

$$P = f(T) + \rho_b \frac{R}{M_b} T \tag{6}$$

or,

$$P = f(T) + \frac{R}{M_b} \rho (1 - w)T \tag{7}$$

where R is the universal gas constant, M_b is the molecular weight of the gas and f(T) is an equation based on the saturated vapor data presented by J.M. Smith [Ref. 9].

Consider the section of wick-wall shown in Figure 20 for an energy balance.

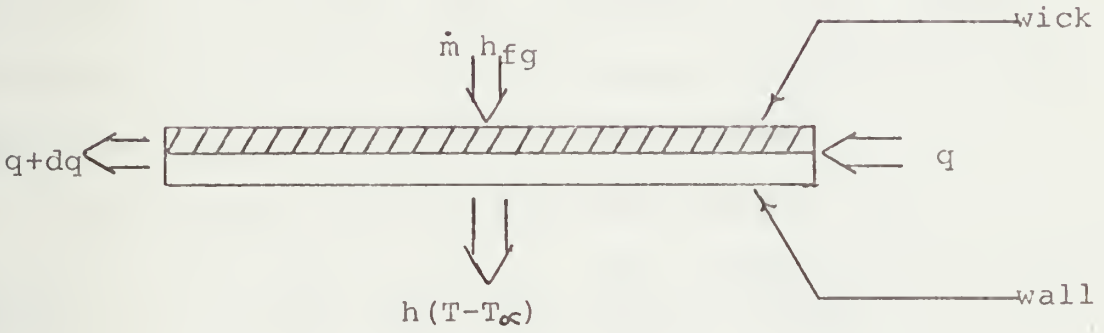

figure 20

Assuming the temperature difference between the wick on the inside of the pipe and the outside of the pipe is negligible in the radial direction:

$$(8)\quad q + \dot{m}\, h_{fg}\, \pi D\, dx = q + dq + h(T - T_\infty)\, \pi\, D_o\, dx$$

where, q is the heat being conducted axially by the pipe, $\dot{m}$ is the rate of condensation of the working fluid per unit area, h_{fg} is the latent heat of condensation of the working vapor, h is the heat transfer coefficient, T_∞ is the ambient temperature and D_o is the outside diameter of the heat pipe.

From Fourier's conduction law:

$$q = -k\, A_p \frac{dT}{dx} \tag{9}$$

where A_p is the cross sectional area of the wick-wall and k is the thermal conductivity in the axial direction of the wick-wall combination. The evaluation of the thermal conductivity, k, and the heat transfer coefficient are developed at a later point in this section.

Substituting equation (9) into equation (8):

$$\frac{d^2T}{dx^2} = \frac{h}{k}(T - T_\infty)\frac{A_s}{L\, A_p} - \frac{\dot{m}\, h_{fg}\, \pi\, D}{k\, A_p} \tag{10}$$

The equations necessary for the development of the analysis are summarized below:

$$-\frac{dP}{dx} + \rho g \sin\theta = \rho V \frac{dV}{dx} + V\frac{d(\rho V)}{dx} + \frac{\pi D}{A_c}\frac{V}{w}\dot{m} \tag{2}$$

$$\dot{m}\frac{\pi D}{A_c} = -\frac{d}{dx}(\rho V) \tag{3}$$

$$V = \frac{1}{(w-1)}\mathfrak{D}\frac{dw}{dx} \tag{5}$$

$$P = f(T) + \frac{R\rho}{M_b}(1-w)T \tag{6}$$

$$\frac{d^2T}{dx^2} = -\dot{m}\frac{h_{fg}\, \pi\, D}{k\, A_p} + \frac{h}{k}(T - T_\infty)\frac{A_s}{L\, A_p} \tag{10}$$

and,

$$\rho = \frac{S}{w} \tag{11}$$

where S is an equation for ρ_a as a function of T, based on the data presented by J.M. Smith [Ref. 9].

As noted in the above equations, the diffusion coefficient, $\mathcal{D}$, has been taken as constant. The diffusion coefficient equation for low pressure is based on the following equation [Ref. 11]:

$$\mathcal{D} = \frac{1.858\ 10^{-3}\ T^{1.5}\ \left[\ \frac{M_1 + M_2}{M_1 M_2}\ \right]}{P\ \sigma_{12}^{\ 2}\ \Omega_D}$$

This indicates that $\mathcal{D}$ does vary somewhat with temperature. However, the above assumption has been made in order to simplify the analysis. A mean diffusion coefficient for the temperature range involved was used in the program.

The following non-dimensional variables were used in the above set of equations:

$$P^* = \frac{P}{P_o}$$

$$\rho^* = \frac{\rho}{\rho_o}$$

$$\rho^* = \frac{S^*}{w}$$

$$V^* = \frac{V}{V_r}$$

where, $$V_r = \frac{\dot{m}_r}{\rho_o}$$

and, $$\dot{m}_r = \frac{Q}{h_{fg}\ A_c}$$

$$m^* = \frac{\dot{m}}{m_r}$$

$$x^* = \frac{x}{L}$$

$$f^* = \frac{f(T)}{P_o}$$

Substituting these into the above equations:

$$(12)\quad \rho^* \sin\theta - \left[\frac{P_o}{\rho_o g L}\right] \frac{dP^*}{dx^*} = \left[\left(\frac{4Q}{\pi D^2 \rho_o h_{fg}}\right)^2 \frac{1}{gL}\right] \left[\rho^* V^* \frac{dV^*}{dx^*} + V^* \frac{d(\rho^* V^*)}{dx^*}\right] + \left[\left(\frac{4Q}{\pi D^2 \rho_o h_{fg}}\right)^2 \frac{1}{gL}\right]\left[\frac{4L}{D}\right] \frac{m^* V^*}{D}$$

$$(13)\quad \dot{m}^* = -\frac{D}{4L} \frac{d}{dx^*} (\rho^* V^*)$$

$$(14)\quad V^* = \frac{1}{(w-1)} \frac{\pi D^2 \rho_o h_{fg} \mathfrak{D}}{4 L Q} \frac{dw}{dx^*}$$

$$(15)\quad P^* = f^*(T) + \left[\frac{R \rho_o T_o}{M_b P_o}\right] \rho^* T^* (1-w)$$

$$(16)\quad \frac{d^2 T^*}{dx^{*2}} = \frac{h L A_s}{k A_p} \left(T^* - \frac{T_\infty}{T_o}\right) - \frac{4 L^2 Q}{D k A_p T_o} \dot{m}^*$$

Substituting for the non-dimensional coefficients in the preceding equations:

$$N_1 = \frac{P_o}{\rho_o g L}$$

$$N_2 = \left[\frac{4Q}{\pi D^2 \rho_o h_{fg}}\right]^2 \frac{1}{gL}$$

$$N_3 = \frac{4L}{D}$$

$$N_4 = \frac{hL}{k} \frac{A_s}{A_p}$$

$$N_5 = \frac{4 L^2 Q}{Dk A_p T_o}$$

$$N_6 = \frac{\pi D^3 \rho_o h_{fg} \mathcal{D}}{16 Q L^2}$$

$$N_7 = \frac{R}{M_b} \frac{\rho_o T_o}{P_o}$$

$$N_3 N_6 = \frac{\pi D^2 \rho_o h_{fg} \mathcal{D}}{4QL}$$

the equations become:

(17) $$\rho^* \sin\theta - N_1 \frac{dP^*}{dx^*} = N_2 \left[\rho^* V^* \frac{dV^*}{dx^*} + V^* \frac{d(\rho^* V^*)}{dx^*}\right]$$

(18) $$\dot{m}^* = -\frac{1}{N_3} \frac{d}{dx^*} (\rho^* V^*)$$

(19) $$V^* = \frac{1}{(w-1)} N_3 N_6 \frac{dw}{dx^*}$$

(20) $$P^* = f^*(T) + N_7 (1+w) P^* T^*$$

(21) $$\frac{d^2 T^*}{dx^{*2}} = N_4 (T^* - T_\infty^*) - N_5 \dot{m}^*$$

Investigating the relative magnitude of the coefficient of the momentum term in equation (17) with respect to the other coefficients for representative values of the operating heat pipe, one finds:

$$N_2 = \left[\frac{4\times10\times3.413}{470\times3.14(1/6)(1/31.1)} \right]^2 \left[\frac{1}{(32.2)(3600)} \right]$$

$$N_2 = 2.4\times10^{-5}$$

A similar investigation of the other terms indicated that N_2 was at least a factor of 10^{-5} times smaller than the value of the other non-dimensional coefficients. This led to the simplifying assumption that the momentum term could be excluded from the analysis without loss of accuracy. The computation of this coefficient was retained in the final program in order to serve as a check on its relative value.

The momentum equation then reduces to a force balance:

$$\rho^* \sin\theta - N_1 \frac{dP^*}{dx^*} = 0 \tag{22}$$

Differentiating equation (20):

$$\frac{dP^*}{dx^*} = \frac{df^*(T)}{dT^*} \frac{dT^*}{dx^*} + N_7 \left(\frac{1-w}{w}\right)\left(S^* + \frac{dS^*}{dT^*} T^*\right) \frac{dT^*}{dx^*} - N_7 \frac{1}{w^2} S^* T^* \frac{dw}{dx^*} \tag{23}$$

Subtracting this from equation (22):

$$(24)\quad \frac{1}{N_1}\frac{S^*}{w}\sin\theta = \frac{df^*}{dT^*}\frac{dT^*}{dx^*} + N_7\left(\frac{1-w}{w}\right)\left(S^* + \frac{dS^*}{dT^*}T^*\right)\frac{dT^*}{dx^*} - N_7\frac{1}{w^2}S^*T^*\frac{dw}{dx^*}$$

Solving equation (24) for $\frac{dw}{dx^*}$ and differentiating:

$$(25)\quad \frac{d^2w}{dx^{*2}} = \left[\frac{w^2}{N_7}G_1 + w(1-w)G_4\right]\frac{d^2T^*}{dx^{*2}} + \left[\frac{w^2}{N_7}G_3 + w(1-w)G_5\right]\left(\frac{dT^*}{dx^*}\right)^2 + \left[\frac{2w}{N_7}G_1 + (1-2w)G_4\right]\frac{dT^*}{dx^*}\frac{dw}{dx^*} + \frac{1}{N_1N_7}\left[-\frac{1}{T^*}\sin\theta\frac{dw}{dx^*} + \frac{w}{T^{*2}}\sin\theta\frac{dT^*}{dx^*}\right]$$

where,

$$G_1 = \frac{df^*}{dT^*}\frac{1}{S^*T^*}$$

$$G_3 = \frac{\frac{d^2f^*}{dT^{*2}}S^*T^* - \frac{df^*}{dT^*}\frac{dS^*}{dT^*}T^* - \frac{df^*}{dT^*}S^*}{(S^*T^*)}$$

$$G_4 = \frac{1}{T^*} + \frac{dS^*}{dT^*}\frac{T^*}{S^*}$$

$$G_5 = \frac{\frac{d^2S^*}{dT^{*2}}S^* + \frac{S^*}{T^*}\frac{dS^*}{dT^*} - \left(\frac{dS^*}{dT^*}\right)^2}{S^{*2}}$$

Substituting equation (18) into equation (21):

$$(26) \qquad \frac{d^2T^*}{dx^{*2}} = N_4(T^* - T_\infty^*) + \frac{N_5}{N_3}\frac{d}{dx^*}(\rho^* V^*)$$

Differentiating equation (19) and substituting into equation (26):

$$(27) \qquad \frac{d^2T^*}{dx^{*2}} = N_4(T^* - T_\infty^*) + N_5N_6\left[\frac{dS^*}{dT^*}\frac{1}{w(w-1)}\frac{dw}{dx^*}\frac{dT^*}{dx^*}\right.$$

$$\left. - \frac{2(w-1)}{w^2(w-1)^2}S^*\left(\frac{dw}{dx^*}\right)^2 + \frac{S^*}{w(w-1)}\frac{d^2w}{dx^{*2}}\right]$$

Substituting equation (25) into equation (27):

$$(28) \qquad G_{10}\frac{d^2T^*}{dx^{*2}} = N_4(w-1)(T^* - T_\infty^*) + G_{11}\frac{dT^*}{dx^*}\frac{dw}{dx^*}$$

$$- G_{12}\left(\frac{dw}{dx^*}\right)^2 + G_{13}\left(\frac{dT^*}{dx^*}\right)^2$$

$$- G_{14}\sin\theta\frac{dw}{dx^*} + G_{15}\sin\theta\frac{dT^*}{dx^*}$$

where,

$$G_{10} = \left[(w-1) - \frac{N_5N_6}{N_7}wS^*G_1 + (w-1)N_5N_6S^*G_4\right]$$

$$G_{11} = \left[\frac{N_5N_6}{w}\frac{dS^*}{dT^*} + \frac{2\,N_5N_6}{N_7}S^*G_1 + N_5N_6\frac{(1-2w)}{w}S^*G_4\right]$$

$$G_{12} = N_5N_6\frac{2w-1}{w^2(w-1)}S^*$$

$$G_{13} = \left[\frac{N_5 N_6}{N_7} w S^* G_3 + N_5 N_6 (w-1) S^* G_5\right]$$

$$G_{14} = \frac{N_5 N_6}{N_1 N_7} \frac{1}{w} \frac{S^*}{T^*}$$

$$G_{15} = \frac{N_5 N_6}{N_1 N_7} \frac{S^*}{T^{*2}}$$

Simplifying equation (25):

$$(29) \quad \frac{d^2 w}{dx^{*2}} = G_{20} \frac{d^2 T^*}{dx^{*2}} + G_{21} \left(\frac{dT^*}{dx^*}\right)^2 + G_{22} \frac{dT^*}{dx^*} \frac{dw}{dx^*}$$

$$- G_{23} \sin\theta \frac{dw}{dx^*} + G_{24} \sin\theta \frac{dT^*}{dx^*}$$

where,

$$G_{20} = \left[\frac{w^2}{N_7} G_1 + w(1-w) G_4\right]$$

$$G_{21} = \left[\frac{w^2}{N_7} G_3 + w(1-w) G_5\right]$$

$$G_{22} = \left[\frac{2w}{N_7} G_1 + (1-2w) G_4\right]$$

$$G_{23} = \left[\frac{1}{N_1 N_7} \frac{1}{T^*}\right]$$

$$G_{24} = \left[\frac{1}{N_1 N_7} \frac{w}{T^{*2}}\right]$$

Equations (28) and (29), along with their associated non-dimensional coefficients, form a set of two, second order, simultaneous non-linear differential equations. As mentioned earlier these equations were solved using the IBM 360/67 computer with a Runge Kutta routine. The entire program was put in double precision to avoid as much machine round off error as possible.

The value of the heat transfer coefficient for natural convection, h, was calculated based on the Nusselt Number, N_{nux} [Ref. 12].

where, $N_{nux} = m(n_{gr} N_{pr})^{.25}$

where, m = .59 for the vertical position

and, m = .525 for the horizontal position

The Nusselt Number for the heat pipe in the horizontal position was found to be 11.59, while for the vertical position the Nusselt Number equalled 67.84. These values were used in the following equation to find the natural convection portion of the heat transfer coefficient, h_c:

$$h_c = \frac{N_{nux}\, k}{x}$$

To this was added the value of the radiation component of the heat transfer coefficient, h_r, resulting in the following final equation:

$$h = h_c + \frac{\sigma \varepsilon (T^4 - T_\infty{}^4)}{(T - T_\infty)}$$

Two values for a condenser temperature of 600° R and an ambient temperature of 540° R are indicative of the relative values used:

horizontal position $h = 1.41$

vertical position $h = 1.00$

In determining the axial thermal conductivity of the wall and saturated wick combination, k, the conductivity of the saturated wick was first determined and then combined with the thermal conductivity of the stainless steel wall in a parallel manner. The determination of the saturated wick thermal conductivity could be viewed as either a parallel or series combination of the wire screen and the working fluid [Ref. 7]. The two values obtained are:

$$k_{series} = \frac{k_s K_L}{\phi k_s + (1 - \phi) k_L} = .296$$

$$k_{parallel} = (1 - \phi)k_s + \phi k_L = 5.80$$

where ϕ is the void fraction in the wick, and is equal to .387.

In assuming the value is that of the parallel case and combining this with the thermal conductivity of the stainless steel wall, the largest possible value of thermal conductivity for the wick-wall combination is obtained. This is what the

designing of the fins was intended to reduce. The axial conductivity used was therefore:

$$k = 15.2 \ \frac{BTU}{hr\ ft\ ^{\circ}F}$$

B. RESULTS

The computer program developed to solve the set of simultaneous, first order, non-linear differential equations is included after Appendix A. Several solutions obtained from this program are included in Figures 21 and 22. The solutions were obtained for a specific heat input by assuming a temperature for the condenser at x equals zero. As a first estimate the condenser temperature from the experimental phase for the same heat input was used. The computer solution indicates in the output the amount of heat the pipe can transfer at this temperature divided by the amount of heat specified as being the input. The condenser temperature was varied until this quotient equalled one.

The analytic solutions shown in Figures 21 and 22 indicate a nearly isothermal condenser. The condenser-evaporator interface is only from 0.01 to 0.2% greater in temperature than the other end of the condenser in these figures.

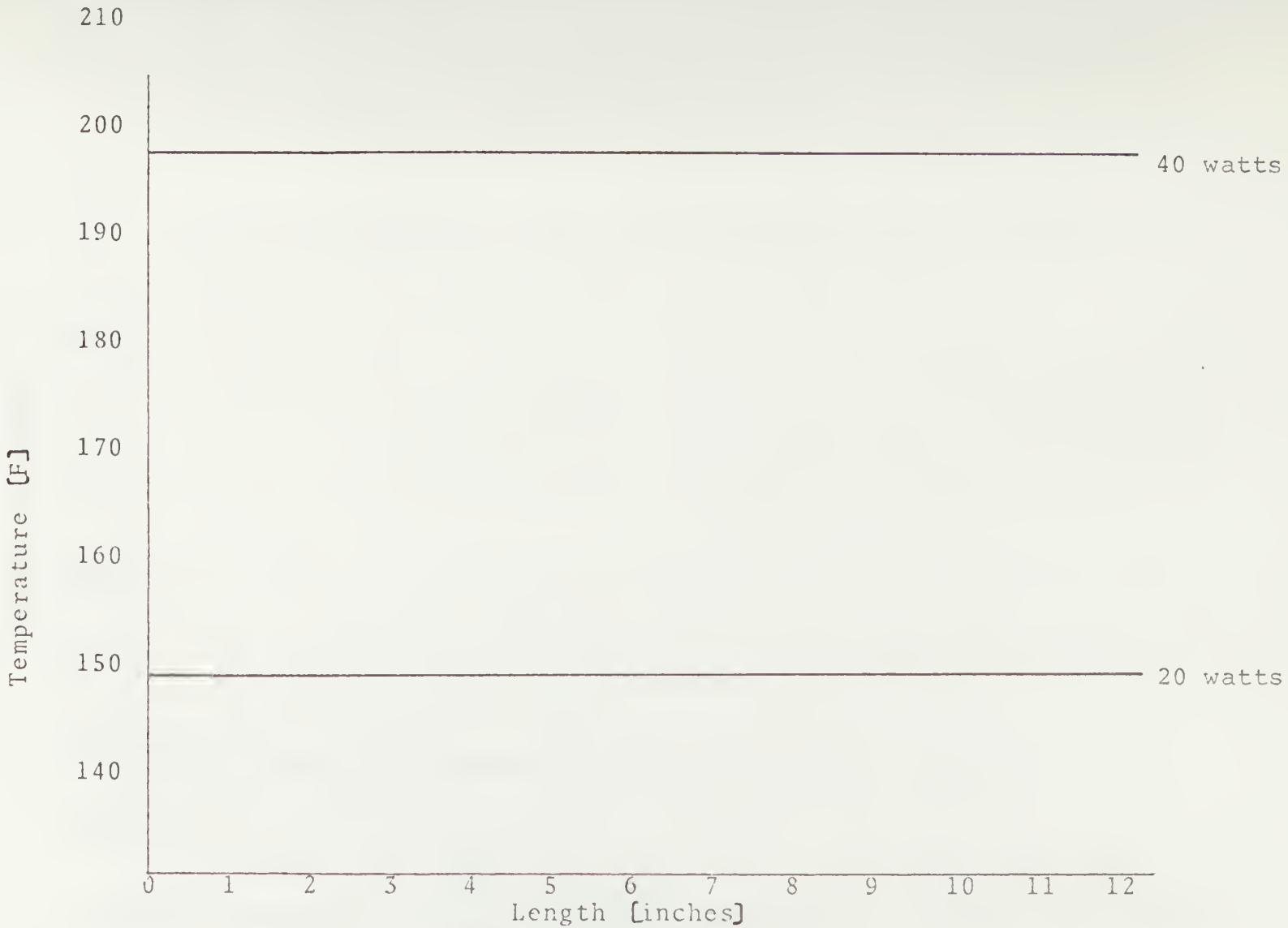

Horizontal position, analytic condenser temperature, methanol and krypton

figure 21

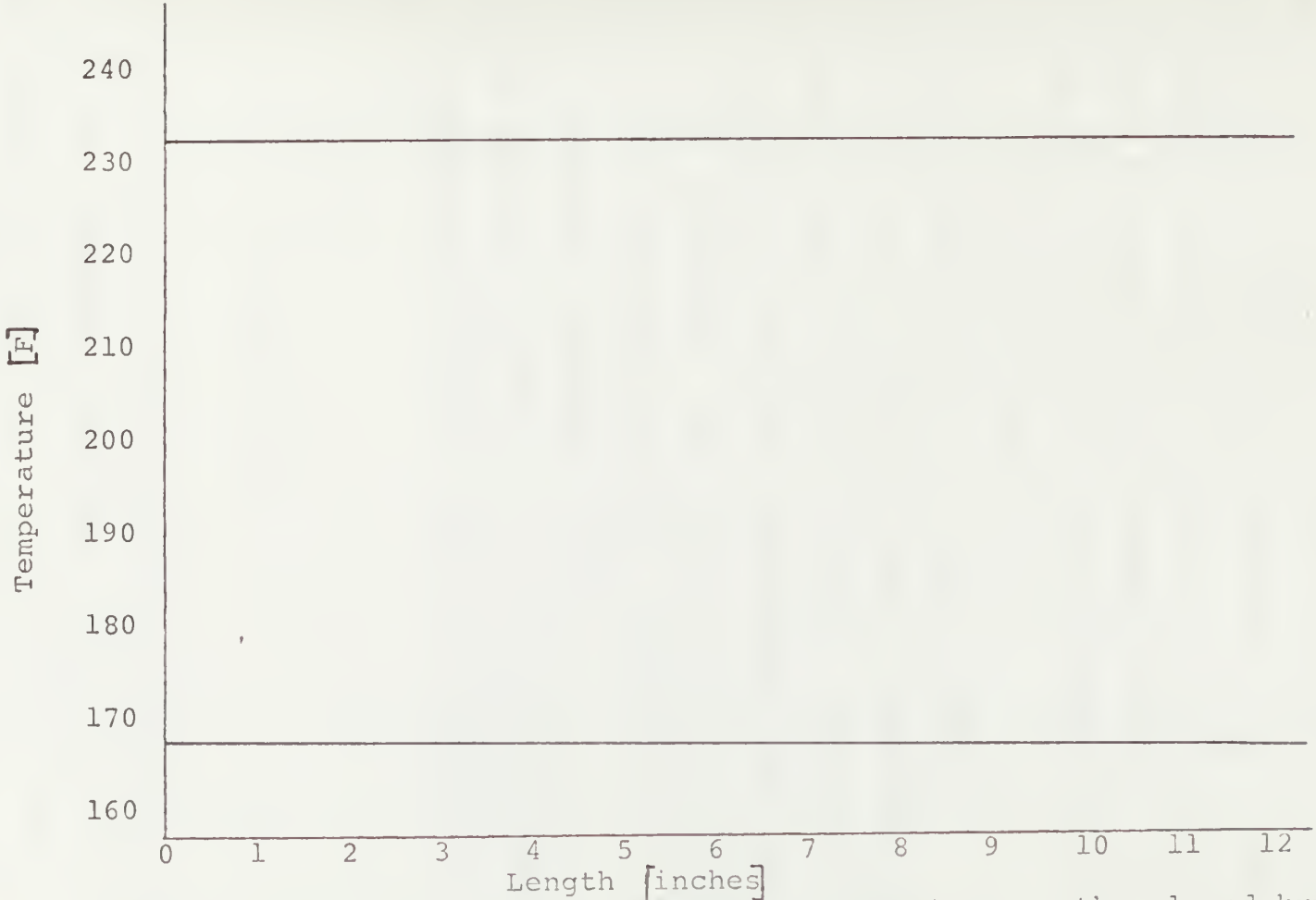

Vertical position, analytic condenser temperature, methanol and krypton

figure 22

V. DISCUSSION

A. COMPARISON OF ANALYSIS AND EXPERIMENT

Figures 12 and 14 present condenser temperature profiles based on the operation of the gas loaded heat pipe. Figures 21 and 22 present the condenser temperature profiles based on the analysis developed in the preceding section. The positions and heat inputs are the same for Figures 12 and 21 and the same for Figures 14 and 22.

The analytic solutions all have higher condenser temperatures than the data obtained from the operating heat pipe for identical heat input and position. The analytic condenser temperatures exceed the operational temperature in °F by 7.2 to 19 percent. The larger difference between the analytic and operational condenser temperature is found in the vertical operating position.

The heat transfer coefficient, h, if increased would reduce the condenser temperature since for a given heat transfer, Q:

$$Q = h(T - T_{\infty})$$

The values of h determined earlier were based on natural convection over a symmetric cylinder. The addition of fins and the removable end plate with its associated flange on the pipe served to disturb the flow over the pipe. This

disturbance of the natural convection over the heat pipe would have more effect in the vertical position where the convection flow travels the length of the pipe. Any such disturbance would tend to allow greater mixing in the convective flow. This would allow a greater amount of heat to be transferred at the same condenser temperature or the original amount of heat transferred at a slightly reduced temperature. This is the effect of increasing the value of h in the preceding equation. Increasing the value of the heat transfer coefficient used in the analytic solution will reduce the condenser temperature obtained. This appears to therefore be one of the reasons for the difference in the analytic and operational condenser temperatures.

The analytic condenser temperature was nearly isothermal as noted earlier. This again differs from the operational condenser temperatures obtained. The condenser temperature decreases with increasing distance from the evaporator in both the analytic and operational solutions. However, the analytic solution did not have as large a decrease as the operating heat pipe did for the vertical position.

The difference in the temperature slopes of the analytic solution and operating heat pipe are not of such magnitude to require the analytic solution to be discarded. In fact, both solutions indicate the absence of any front. Therefore, the assumptions of negligible viscous and momentum forces in the analysis are justified.

The analysis is unable to give any insight into the possibility of stratification in a horizontal gas loaded heat pipe, except to confirm the lack of any vapor gas front. The possibility of stratification in an operating heat pipe cannot be overlooked. The design of the gas reservoir may require alteration to allow the stratified gas to flow in and out with heat input and pressure changes.

The heat transfer characteristic of a gas loaded heat pipe with stratification will differ from the flat front and diffuse models discussed earlier. The stratified heat pipe may produce some of the characteristics of the diffuse front model with the front turned 90° in the pipe.

B. RECOMMENDATIONS

Further investigation with the computer program has indicated a heat pipe of different dimensions from that used in this experiment may yield more interesting results. A longer pipe of smaller diameter with a higher heat transfer coefficient produces a marked vapor-gas front in the analytic solution. With such a diffuse front the rotation of the pipe through 90° could be attempted to observe the gravitational effect on the vapor-gas front.

In addition, other inert gases could be introduced into the existing heat pipe in place of krypton. Lighter gases may allow the vapor-gas front to become more apparent while

also providing a comparison for the data in this work concerning the possibility of stratification. The use of liquid crystals could continue to provide insight into this phenomenon.

APPENDIX A

SAMPLE CALCULATIONS OF ERROR ANALYSIS

$$Q = I^2R = \frac{V^2}{R}$$

$$W_Q = \left[\left(\frac{2V}{R} W_v\right)^2 + \left(\frac{-V^2}{R^2} W_R\right)^2\right]^{1/2}$$

where V is the voltage, R is the resistance, W_R is the error bound in the resistance and W_V is the error bound in the voltage.

Dividing both sides by Q:

$$\frac{W_Q}{Q} = \left[\left(\frac{2}{V} W_v\right)^2 + \left(\frac{W_R}{R}\right)^2\right]^{1/2}$$

$$\frac{W_Q}{Q} = \left[\left(\frac{2}{10.845} \times .05\right)^2 + \left(\frac{.003}{2.013}\right)^2\right]^{1/2}$$

$$\frac{W_Q}{Q} = 0.0093$$

$$\frac{W_Q}{Q} = 0.93\ \%$$

Quantity		Error bound
T	Temperature	± 0.5 F
P	Pressure	± 0.4 psia
Q	Heat input	± 0.93%
L	Length	± 0.004 feet
D	Diameter	± 0.0004 feet
$\mathfrak{D}$	Diffusion coefficient	± 1.84%
h	Heat transfer coefficient	± 2.8%
g	Gravity	± 0.01 ft/sec^2
h_{fg}	Latent heat of vaporization	± 0.03 BTU/lbm
σ	Surface tension	± 2×10^{-5} lb/ft
ρ	Density	± 0.01 lbm/ft^3
ν	Kinematic viscosity	± 3×10^{-4} ft^2/hr
V	Voltage	± 0.05 volts
R	Resistance	± 0.003 ohms
Ø	Void fraction of wick	± 1.0%
m	Condensation rate	± 2.4%

```
      IMPLICIT REAL*8 (A-H,O-Z)
      COMMON/BLOCK1/XN1,XN2,XN3,XN4,XN5,XN6,XN7,XN8,RMAB,TO,PO,AF,BF,CF
     1,DF,EF,TIS,THETA
      DIMENSION VAR(5),DER(5),Y(6,1001),YY(1001)
      SS(X)=DF*DEXP(AF/((TO*X)**2)+BF/(TO*X)+CF)*X**EF/PO
C
CC    THE FIRST DERIVATIVE OF SS AND FS
C
      SSP(X)=DF*(DEXP(AF/((TO*X)**2)+BF/(TO*X)+CF)/PO)*X**(EF-ONE)*(EF
     1-TWO*AF/((TO*X)**2)-BF/(TO*X))
      FS(X)=DEXP(AF/((TO*X)**2)+BF/(TO*X)+CF)/PO
      FSP(X)=-DEXP(AF/((TO*X)**2)+BF/(TO*X)+CF)*(TWO*AF/(TO*X)+BF)
     1/(PO* TO*X **2)
      ZERO=0.0D0
      PRINT 1
    1 FORMAT(1H1)
      ONE=1.0D0
      TWO=2.0D0
      THR=3.0D0
      FOR=4.0D0
      SXT=16.0D0
      R=1545.D0
      GC=32.2D0
      SISF=144.D0
      SPH=3600.D0
C
CC    READ IN PARAMETERS OF HEAT PIPE PROBLEM
C
      READ 1005, XL,D,AS,AP,CONK
      READ 1002, RMA,RMB
      READ 1003, PO, TO, TINF
      READ 1004, Q,GRAV,HTC,THETA
      READ 1003,AF,BF,CF
      CS=1.218D0
      EF=-.852D0
      RHO=CS*PO*TO**EF*FS(ONE)+RMB*PO*SISF*(ONE-FS(ONE))/R/TO
      RHE=RHO
      DF=CS*PO*TO**EF/RHO
      TIS=TINF/TO
      QW=Q/3.413D0
C
CC    CALCULATE THE DIFFUSION COEFFICIENT
C
      DIFF=DSQRT(TO**3)/(PO*(2837.143844D0-1.488620348D0*TO))
C
CC    CALCULATE THE LATENT HEAT OF VAPORIZATION
C
      HFG=517.312D0+.127429D0*TO+.652248D-05*TO**2-.551138D-06*TO**3
```

```
      PRINT 2001
 2001 FORMAT(4X,11HLENGTH (FT),3X,13HDIAMETER (FT),4X,9HAS (SQFT),6X,
     19HAP (SQFT),5X,13HK (B/HR/FT/F))
      PRINT 2002,XL,D,AS,AP,CONK
 2002 FORMAT(2X,5D15.8)
      PRINT 2003
 2003 FORMAT(///9X,2HMA,13X,2HMB,8X,11HHFG (B/LBM),3X,14HDIFF (SQFT/HR))
      PRINT 2004, RMA,RMB,HFG,DIFF
 2004 FORMAT(7X,F6.2,9X,F6.2,7X,F8.2,4X,D15.8)
      PRINT 2005
 2005 FORMAT(///2X,14HRHO (LBM/CUFT),4X,13HPO (LBF/SQIN),4X,
     110HTO (DEG R),4X,12HTINF (DEG R))
      PRINT 2006, RHO,PO,TO,TINF
 2006 FORMAT(2X,D15.8,2X,D15.8,4X,F7.1,7X,F7.1)
      PRINT 2007
 2007 FORMAT(///4X,10HQ (BTU/HR),6X,9HQ (WATTS),4X,13HG (FT/SEC**2),1X,
     115HH (B/HR/SQFT/F),3X,11HTHETA (DEG))
      PRINT 2008,Q,QW,GRAV,HTC,THETA
 2008 FORMAT(6X,5(F7.2,8X))
      PRINT 2009
 2009 FORMAT(///8X,2HAF,13X,2HBF,13X,2HCF,10X,
     142H (COEFFICIENTS FOR VAPOR PRESSURE FORMULA))
      PRINT 2013, AF,BF,CF
 2013 FORMAT(2X,3(D13.6,2X))
      PI=3.141593D0
      THETA=THETA*PI/180.0D0
C     CALCULATE NONDIMENSIONAL COEFFICIENTS
      XN1=(PO/(RHO*GRAV*XL))*GC*SISF
      XN2=((FOR*Q/(PI*(D**2)*RHE*HFG*SPH))**2)/(GRAV*XL)
      XN3=(RHE/RHO)*(FOR*XL/D)
      XN4=(HTC*XL/CONK)*(AS/AP)
      XN5=FOR*(XL**2)*Q/(D*CONK*AP*TO)
      XN6=(PI*(D**3)*RHO*HFG*DIFF/(SXT*Q*(XL**2)))*SPH
      XN7=(R/RMB)*(RHO*TO/PO)/SISF
      XN8=XN6*XN3
      PRINT 2020
      PRINT 2021,XN1,XN2,XN3,XN4,XN5,XN6,XN7,XN8
 2020 FORMAT(/6X,2HN1,12X,2HN2,12X,2HN3,12X,2HN4,12X,2HN5,12X,2HN6,
     112X,2HN7,12X,2HN8)
 2021 FORMAT(8(2X,D12.6))
      RMAB=RMA/RMB
C
C     INITIAL CONDITIONS
C
      X=ZERO
      DER(1)=.001D0
      DX=DER(1)
      VAR(1)=ZERO
```

```
      VAR(2)=ONE
      VAR(3)=DSIN(THETA)/(FSP(ONE)+XN7*(ONE-SS(ONE)-SSP(ONE)+SSP(ONE)/
     1SS(ONE)))/XN1
      VAR(4)=SS(ONE)
      VAR(5)=ZERO
      N1=4
C
C     INTEGRATION INCREMENT
C
      M=1000
      M1=M+1
      DO 10 J=1,N1
   10 Y(J,1)=VAR(J+1)
      Y(5,1  )=FS(VAR(2))+XN7*(ONE-VAR(4))*VAR(2)*SS(VAR(2))/VAR(4)
      Y(6,1)=ONE
      YY(1)=ZERO
      PRINT2010
      PRINT 2011, VAR(1),(Y(J,1),J=1,6),YY(1)
 2010 FORMAT(////4X,2HX*,9X,2HT*,14X,7HDT*/DX*,12X,1HW,15X,6HDW/DX*,11X,
     12HP*,14X,4HRHO*,13X,5HMDOT*/)
 2011 FORMAT(2X,F6.3,7(2X,D15.8))
      K=10
      DO 11 I=1,M
      CALL RK1 (VAR,DER,N1)
      DO 12 J=1,N1
   12 Y(J,I+1)=VAR(J+1)
C  P*=Y(5,2)
C  RHO*=Y(6,I)
      Y(5,I+1)=FS(VAR(2))+XN7*(ONE-VAR(4))*VAR(2)*SS(VAR(2))/VAR(4)
      Y(6,I+1)=SS(VAR(2))/VAR(4)
      KK=I+1
      YY(KK)=VAR(2)-TIS
      SMS=(XN4/XN5)*SUM(1,KK,YY,DX)-(VAR(3)-Y(2,1))/XN5
      IF((I/K).EQ.1) GO TO 20
      GO TO 11
   20 PRINT 2011, VAR(I),(Y(J,I+1),J=1,6),SMS
      K=K+10
   11 CONTINUE
C
C     CALCULATE THE RATIO OF ACTUAL HEAT TRANSFERRED TO HEAT INPUT AND
C     THE LBM MASS OF KRYPTON
C
      SMTOT=XN3*SMS
      DO 14 I=1,1001
   14 YY(I)=Y(6,I)*(ONE-Y(3,I))
      BMASS=(PI*D**2/FOR)*XL*RHO*SUM(1,1001,YY,DX)
      PRINT 2030, SMTOT,BMASS
 2030 FORMAT(/////10X,7HMTOT* =,F8.5,15X,17HMASS OF KRYPTON =,D13.6,
```

```
     12X,3HLBM)
1002 FORMAT(2D15.8)
1003 FORMAT(3D15.8)
1004 FORMAT(4D15.8)
1005 FORMAT(5D15.8)
      STOP
      END
```

```
      SUBROUTINE DERS(VAR,DER,K)
C
      IMPLICIT REAL*8 (A-H,O-Z)
      COMMON/BLOCK1/XN1,XN2,XN3,XN4,XN5,XN6,XN7,XN8,RMAB,TO,PO,AF,BF,CF
     1,DF,EF,TIS,THETA
      DIMENSION VAR(5),DER(5)
      FS(X)=DEXP(AF/((TO*X)**2)+BF/(TO*X)+CF)/PO
      FSP(X)=-DEXP(AF/((TO*X)**2)+BF/(TO*X)+CF)*(TWO*AF/(TO*X)+BF)
     1/(PO* TO*X **2)
      SS(X)=DF*DEXP(AF/((TO*X)**2)+BF/(TO*X)+CF)*X**EF/PO
      SSP(X)=DF*(DEXP(AF/((TO*X)**2)+BF/(TO*X)+CF)/PO)*X**(EF-ONE)*(EF
     1-TWO*AF/((TO*X)**2)-BF/(TO*X))
C
CC    THE SECOND DERIVATIVE OF SS AND FS
C
      FSPP(T)=FS(T)*(SIX*AF/TO**2/T+TWO*BF/TO)/T**3
     1-FSP(T)*(TWO*AF/TO**2/T+BF/TO)/T**2
      SSPP(T)=SSP(T)*(EF-ONE-BF/TO-TWO*AF/TO**2/T)/T
     1+SS(T)*(FOR*AF/TO**2/T+BF/TO)/T**3
      ZERO=0.0D0
      HAF=0.5D0
      ONE=1.0D0
      TWO=2.0D0
      THR=3.0D0
      FOR=4.0D0
      SIX=6.0D0
      T=VAR(2)
      W=VAR(4)
      G1=FSP(T)/SS(T)/T
      G3=(FSPP(T)*SS(T)*T-FSP(T)*SS(T)-FSP(T)*SSP(T)*T)/(SS(T)*T)**2
      G4=(ONE+SSP(T)*T/SS(T))/T
      G5=(SSPP(T)/SS(T)-(SSP(T)/SS(T))**2-ONE/T**2)
      G10=((W-ONE)-XN5*XN6*W*G1*SS(T)/XN7+(W-ONE)*XN5*XN6*G4*SS(T))
      G11=XN5*XN6*SSP(T)/W+TWO*XN5*XN6*G1*SS(T)/XN7+XN5*XN6*(ONE-TWO*W)
     1*G4*SS(T)/W
      GG=ONE-W
      G12=ZERO
      IF (GG.GT.1.D-20)
     1G12=XN5*XN6*SS(T)*(TWO*W-ONE)/((W-ONE)*W**2)
      G13=XN5*XN6*W*SS(T)*G3/XN7-XN5*XN6*(W-ONE)*G5*SS(T)
      G14=XN5*XN6*SS(T)/(XN1*XN7*W*T)
      G15=XN5*XN6*SS(T)/(XN1*XN7*T*T)
      G20=G1*W**2/XN7+W*(ONE-W)*G4
      G21=G3*W**2/XN7+W*(ONE-W)*G5
      G22=TWO*G1*W/XN7+(ONE-TWO*W)*G4
      G23=ONE/(XN1*XN7*T)
```

```
      G24=W/(XN1*XN7*T**2)
      DER(2)=VAR(3)
      DER(3)=(XN4*(W-ONE)*(T-TIS)+G11*VAR(3)*VAR(5)-G12*VAR(5)**2
     1+G13*VAR(3)**2-(G14*VAR(5)-G15*VAR(3))*DSIN(THETA))/G10
      DER(4)=VAR(5)
      DER(5)=G20*DER(3)+G21*VAR(3)**2+G22*VAR(3)*VAR(5)
     1+(G24*VAR(3)-G23*VAR(5))*DSIN(THETA)
      RETURN
      END
```

```
      SUBROUTINE RK1 (VAR,DER,N)
C
      IMPLICIT REAL*8 (A-H,O-Z)
      DIMENSION VAR(5),DER(5),TEMP(25)
      HAF=.5D0
      TWO=2.0D0
      SIX=6.0D0
      M1=N+1
      M3=2*N+2
      M5=3*N+3
      M7=4*N+4
      DO 5 I=1,M1
    5 TEMP(I)=VAR(I)
      K=0
      CALL DERS(VAR,DER,K)
      DO 6 I=1,N
    6 TEMP(M1+I)=DER(1)*DER(I+1)
      DO 7 I=2,M1
    7 VAR(I)=TEMP(I)+HAF*TEMP(M1+I-1)
      VAR(1)=TEMP(1)+HAF*DER(1)
      K=1
      CALL DERS(VAR,DER,K)
      DO 8 I=1,N
    8 TEMP(M3+I)=DER(1)*DER(I+1)
      DO 9 I=2,M1
    9 VAR(I)=TEMP(I)+HAF*TEMP(M3+I-1)
      VAR(1)=TEMP(1)+HAF*DER(1)
      K=1
      CALL DERS(VAR,DER,K)
      DO 10 I=1,N
   10 TEMP(M5+I)=DER(1)*DER(I+1)
      DO 11 I=2,M1
   11 VAR(I)=TEMP(I)+TEMP(M5+I-1)
      VAR(1)=TEMP(1)+DER(1)
      K=2
      CALL DERS(VAR,DER,K)
      DO 12 I=1,N
   12 TEMP(M7+I)=DER(1)*DER(I+1)
      DO 13 I=2,M1
   13 VAR(I)=TEMP(I)+(TEMP(M1+I-1)+TWO*TEMP(M3+I-1)
     1+TWO*TEMP(M5+I-1)+TEMP(M7+I-1))/SIX
      K=2
      CALL DERS(VAR,DER,K)
      RETURN
      END
```

```
      REAL FUNCTION SUM*8(N,M,A,H)
C
      IMPLICIT REAL*8 (A-H,O-Z)
      DIMENSION A(1001)
C
C     SIMPSON'S ONE THIRD INTEGRATION
C
      IF((M-N).EQ.0) GO TO 1
      IF((M-N).EQ.1) GO TO 2
      SUM=0.0D0
      I=N
    3 IF(I.EQ.M) RETURN
      IF(I.EQ.(M-1)) GO TO 4
      SUM=SUM+(A(I)+A(I+2)+4.0D0*A(I+1))*H/3.0D0
      I=I+2
      GO TO 3
    4 SUM=SUM+(A(M-1)+A(M))*H/2.0D0
      RETURN
    1 SUM=0.0D0
    2 SUM=(A(N)+A(M))*H/2.0D0
      RETURN
      END
```

LIST OF REFERENCES

1. Gaugler, R. S., Heat Transfer Device, U.S. Patent 2, 350, 348, 6 June 1944.

2. General Electric Technical Information Series, nbr. 61sd114, On the Surface-Tension Pumping of Liquids, or, a Possible Role of the Candlewick in Space Exploration, by L. Trefethen, February 1962.

3. Grover, G.M., et. al., "Structures of Very High Thermal Conducatnce," Journal of Applied Physics, v. 35, p. 1990-1991, 1964.

4. U.K. Atomic Energy Authority, AEREM 1610, Experimental Heat Pipes, by K. F. Bainton, 1965.

5. RCA, "Heat Pipe Sweats to Harness Nuclear Reactor Heat," Electromechanical Design, v. 11, 1967.

6. Bienert, W., Heat Pipes for Temperature Control, paper presented at Intersociety Energy Conversion Engineering Conference, 4th, Washington, D.C., 1969.

7. NASA Contract Report 2018, Theory and Design of Variable Conductance Heat Pipes, by B.D. Marcus, April 1972.

8. Woodard, J.S., The Operation of Rotating Non-Cupillary Heat Pipes, Masters Thesis Naval Postgraduate School, 1972.

9. Smith, J.M., "Thermodynamic Properties of Methyl Alcohol," Chemical Engineering Progress.

10. Meyer, J.F., Mac Kenzie, D.K., and Wirzburger, A.M., Thermal Mapping of Surface Temperature Using Cholesteric Liquid Crystals, Mechanical Engineering Laboratory Report, Naval Postgraduate School, 9 June 1972.

11. Reid, R.C. and Sherwood, T.K., The Properties of Gases and Liquids, 2d ed., P. 537, McGraw-Hill, 1958.

12. Chapman, A.J., Heat Transfer, 2d ed., Pp. 361-368, Macmillan, 1967.

INITIAL DISTRIBUTION LIST

		No. Copies
1.	Defense Documentation Center Cameron Station Alexandria, Virginia 22314	2
2.	Library, Code 0212 Naval Postgraduate School Monterey, California 93940	2
3.	Assoc. Professor M. Kelleher, Code 59KK Department of Mechanical Engineering Naval Postgraduate School Monterey, California 93940	2
4.	Department of Mechanical Engineering Naval Postgraduate School Monterey, California 93940	1
5.	Lcdr K.E. Reynolds USN Naval Shipyard U.S. Naval Station Charleston, South Carolina	1

ecurity Classification

DOCUMENT CONTROL DATA - R & D

ecurity classification of title, body of abstract and indexing annotation must be entered when the overall report is classified)

TING ACTIVITY (Corporate author)

Naval Postgraduate School
Monterey, California 93940

2a. REPORT SECURITY CLASSIFICATION
Unclassified

2b. GROUP

TITLE

nestigation of the Performance of a Gas-Loaded Variable
oductance Heat Pipe

IPTIVE NOTES (Type of report and, inclusive dates)

ineer's Degree; December 1972

R(S) (First name, middle initial, last name)

eth Earl Reynolds

T DATE	7a. TOTAL NO. OF PAGES	7b. NO. OF REFS
ember 1972	81	12

RACT OR GRANT NO.	9a. ORIGINATOR'S REPORT NUMBER(S)
ECT NO.	
	9b. OTHER REPORT NO(S) (Any other numbers that may be assigned this report)

RIBUTION STATEMENT

proved for public release; distribution unlimited.

LEMENTARY NOTES	12. SPONSORING MILITARY ACTIVITY
	Naval Postgraduate School Monterey, California 93940

RACT

A variable conductance heat pipe was designed and constructed to udy the performance characteristics of the gas loaded heat pipe ch particular emphasis on the effect of gravity. Heat inputs were ried from 10 to 50 watts and the operating position of the pipe s varied from horizontal to vertical with the condenser above the aporator. Condenser temperature profiles are presented for rious heat inputs and positions for the conventional and gas aded heat pipe. The possibility of stratification in a rizontal heat pipe operating with a non-condensable gas that has larger molecular weight than the working fluid is discussed based observations presented.

Additionally, a one dimensional analysis was formulated and used compare with the experimental results. The results show a good reement between theory and experiment, indicating that the veloped mathematical model adequately describes the physical tuation.

FORM 1473 (PAGE 1)
1 NOV 65
101-807-6811

Security Classification

A-31408

KEY WORDS	LINK A		LINK B		LINK C	
	ROLE	WT	ROLE	WT	ROLE	WT
gas loaded heat pipe						
analysis of gas loaded heat pipe						
variable conductance heat pipe						
heat pipe stratification						

141762

Thesis
R3696
c.1

Reynolds
Investigation of the performance of a gas-loaded variable conductance heat pipe.